Article

Programming biological communication between distinct membraneless compartments

Bo-Tao Ji[1,2], He-Tong Pan ●[1,2], Zhi-Gang Qian ●[1] ✉ & Xiao-Xia Xia ●[1] ✉

Distinct membraneless organelles within cells collaborate closely to organize crucial functions. However, biosynthetic communicating membraneless organelles have yet to be created. Here we report a binary population of membraneless compartments capable of coexistence, biological communication and controllable feedback under cellular environmental conditions. The compartment consortia emerge from two orthogonally phase-separating proteins in a cell-free expression system. Their appearance can be programmed in time and order for on-demand delivery of molecules. In particular, the consortia can sense, process and deliver functional protein cargo in response to a protease message or a DNA message that encodes the protease. Such DNA-based molecular programs can be further harnessed by installing a feedback loop that controls the information flow at the messenger RNA level. These results contribute to understanding crosstalk among membraneless organelles and provide a design principle that can guide construction of functional compartment consortia.

Cells precisely regulate their biological functions through the organization of cellular components into physically separated compartments. This spatial discontinuity underscores the vital importance of communication between diverse compartments for cellular functions[1,2]. In addition to classical functional compartments surrounded by membranes, membraneless organelles (MLOs) formed through liquid–liquid phase separation (LLPS), leveraging their highly dynamic nature, aid in the extensive functionality of metabolic processes and signaling pathways[3–5]. It has been suggested that crosstalk of shared protein components between MLOs is essential in cell-fate decisions[6,7]. However, our understanding of the vital importance of inter-MLO crosstalk is still limited.

Until now, it remains inherently challenging to recapitulate or reprogram the multiple populations of MLOs within cells[8,9]. Despite notable endeavors in chemical construction of multiphasic membraneless compartments using synthetic polymers[10–13], DNA molecules[14,15]

and amylose derivatives[16], their inherent limitations may restrict the exploration of biological communication and collaboration, such as the DNA–mRNA–protein information flow to orchestrate complex biochemical reactions and regulatory networks. Therefore, new design principles are necessary to expand the toolset for constructing a consortia of MLOs that can coexist and cooperate to perform biological tasks under cellular environmental conditions.

We envision that synthetic biology with cell-free systems is a useful in vitro tool for the construction of coexisting and cooperating MLOs. Because of the inherent biologically relevant feature, cell-free expression (CFE) systems mimic the cellular environmental conditions, retain all the biomolecular components necessary and sufficient to complete the DNA to functional protein transition and reduce interference from other cellular compartments or interactions typically present when working with whole cells[17,18]. It is also reasoned that using cell-free synthetic biology to construct multiple MLOs will help understand the

[1]State Key Laboratory of Microbial Metabolism, Joint International Research Laboratory of Metabolic & Developmental Sciences, and School of Life Sciences and Biotechnology, Shanghai Jiao Tong University, Shanghai, People's Republic of China. [2]These authors contributed equally: Bo-Tao Ji, He-Tong Pan. ✉e-mail: zgqian@sjtu.edu.cn; xiaoxiaxia@sjtu.edu.cn

cell's 'division of labor' choice and provide new insights into how the resulting MLOs could stably coexist without merging and cooperate to perform tasks.

Here, we report the construction of a binary population of coexisting and biologically communicating membraneless compartments in a bacterial *Escherichia coli* cell lysate-based expression system. The compartment consortia were based on two intrinsically disordered proteins: the pole-organizing protein Z (PopZ) that regulates asymmetric cell division by forming microdomains at the poles of the bacterium *Caulobacter crescentus*[19,20] and a resilin-like protein R32 capable of forming membraneless compartments in recombinant *E. coli* cells[21]. Their autonomous formation and immiscibility are realized under the cellular environmental conditions without external addition of any macromolecular crowders. Intriguingly, the appearance of the distinct compartments can be programmed in time and order for on-demand crosstalk. Moreover, we demonstrate that the compartment consortia can sense, process and deliver functional protein cargo in response to protein or DNA messages and the DNA-based molecular program can be further harnessed by installing a feedback loop for controllable information flow.

Results

Design and construct distinct membraneless compartments

We were inspired by the cell's 'division of labor' choice of multiple orthogonal MLOs and sought to recapitulate this feat in the biologically relevant CFE system. However, it is rather difficult to create immiscible and biologically communicating membraneless compartments because of the challenges in independently controlling homotypic and heterotypic interactions that direct the underlying components to form discrete condensed phases[8,22]. As a minimalistic model, a binary population of such compartments should ideally meet the following criteria: (1) a pair of intrinsically disordered proteins interact with dominant homotypic interactions over heterotypic interactions; (2) the compartment consortia provide desirable permeability toward specific biomolecules; and (3) compartment consortium formation is programmable in time and order and essentially orthogonal to other entity functioning. To this end, we chose PopZ and R32 because of the absence of homologs in the model bacterial *E. coli* cell lysate[23,24] and their tendency to form liquid-like condensates through different mechanisms. It has been suggested that PopZ assembly into membraneless compartments is driven by its helical oligomerization domain[25], whereas R32 condensation is directed by its unique repetitive amino acid composition[21].

Initially we studied whether PopZ protein compartments could arise from de novo expression of the *popZ* gene in the *E. coli* cell extract-based CFE system (Fig. 1a). Confocal microscopy revealed the formation of spherical compartments upon incubation of the CFE system at 30 °C for 4 h, whereas such compartments were absent in expression of the GFP control (Fig. 1b). To visualize the PopZ condensates and evaluate the formation kinetics, we added spiked DNA templates, which encoded untagged and GFPmut3-tagged PopZ at a predetermined molar ratio of 13.3:1 (Supplementary Fig. 1) in the CFE mixture. Surprisingly, an extremely rapid formation of PopZ compartments occurred within 15 min of CFE (Fig. 1c), reflecting robust protein accumulation to reach concentrations surpassing its condensation threshold. Here, the threshold concentration was estimated to be ~0.25 μM (Supplementary Fig. 2), which was comparable to the values determined in reconstitutions[25]. We also observed an increase in the compartment size with an extended CFE time at the individual (white arrowheads in Fig. 1c) and population (Fig. 1d) levels. This trend may result from growth of the existing compartments into larger ones or fusion of neighboring compartments (Fig. 1e), which supported that the formed compartments were liquid-like. Moreover, the evolving micron-sized compartments can be readily dissolved upon dilution of the CFE mixtures (Supplementary Fig. 3). Together, these results demonstrated the appreciable LLPS capability of PopZ in the CFE system

and prompted us to use it for compartment consortium construction in subsequent studies.

To construct a binary population of membraneless compartments, we sought to supplement the above *popZ* expression mixture with resilin-like protein R32 (Fig. 2a). We first studied whether the resilin-like protein could spontaneously form compartments in the fresh CFE mixture. Therefore, the histidine-tagged R32 (His−R32) protein was biosynthesized, purified (Supplementary Fig. 4) and conjugated with tetramethylrhodamine isothiocyanate (TRITC) for fluorescence imaging. Interestingly, His−R32 spiked with its TRITC conjugate formed liquid compartments at a threshold protein concentration of 0.6 mg ml^{-1} (Supplementary Fig. 5) and this threshold could be significantly lowered with the addition of a small amount of Ni^{2+}. This indicated that the Ni^{2+} ion facilitates condensation of the His−R32 protein, which is attributed to reinforced molecular interactions resulting from high affinity of the His-tag for the metal ion. Then, we monitored the mixture containing the spiked His−R32 protein and *popZ* template before and after CFE. As expected, the R32 compartments formed in the initial CFE mixture witnessed the emergence of another population of PopZ compartments (Fig. 2b and Extended Data Fig. 1). We found that the two compartment populations selectively enrich their respective constituents (Fig. 2c), suggesting desirable orthogonality in the protein condensation. The formation of such orthogonal compartments may be directed by the inherent competition between homotypic and heterotypic interactions of the constituent proteins[8]. Analysis of compartment dynamics by photobleaching revealed that the majority of fluorescence (~92%) was recovered in single R32 compartments (Fig. 2d), reflecting their highly fluidic nature. However, slow and slight fluorescence recovery was observed for the PopZ compartments, indicating that the PopZ molecules may exist in a kinetically arrested state. We also found that the compartment consortia repelled DNA template of the CFE (Extended Data Fig. 2) and the gene transcription and translation machinery proteins (Extended Data Fig. 3). Notably, the compartment consortium formation was compatible with functioning of the CFE system to generate another model blue fluorescent protein mTagBFP2, which was evenly distributed in the system as expected (Fig. 2e). Moreover, formation of the compartment consortia could be confined to occur in lipid-enclosed protocells containing the CFE mixtures of interest (Extended Data Fig. 4). Overall, these results supported the autonomous formation of a binary population of membraneless compartments that are compositionally and dynamically distinct and compatible to functioning of the CFE system.

Small-molecule delivery between distinct compartments

The selective uptake of substances by membraneless compartments has a decisive role in the transmission of signaling molecules[6] and will form an important basis for the intercompartment communication that we aim to achieve. Thus, we investigated whether our compartment consortia would selectively uptake certain small molecules. We surmise that the PopZ compartments may enrich substances with positive charges because this protein's central intrinsically disordered region is rich in negatively charged amino acids[25] and the R32 compartments prefer substances with negative charges because of the presence of positively charged arginine and aromatic tyrosine residues in each repetitive unit[26]. To verify this hypothesis, we studied whether the two compartments could selectively enrich charged fluorescent molecules. As expected, the individual PopZ compartments enriched the positively charged rhodamine 6G (Rh 6G) and the moderately negatively charged sulforhodamine B (SRh B) but not the highly negatively charged pyranine; in contrast, the R32 compartments preferred pyranine and SRh B to Rh 6G (Extended Data Fig. 5). In addition, pyranine and SRh B did not affect the capability of the R32 protein to form compartments (Supplementary Fig. 6) and Rh 6G did not affect the formation, size or liquid-like property of the evolving PopZ compartments (Supplementary Fig. 3). Moreover, fluorescence of these two dyes was insensitive
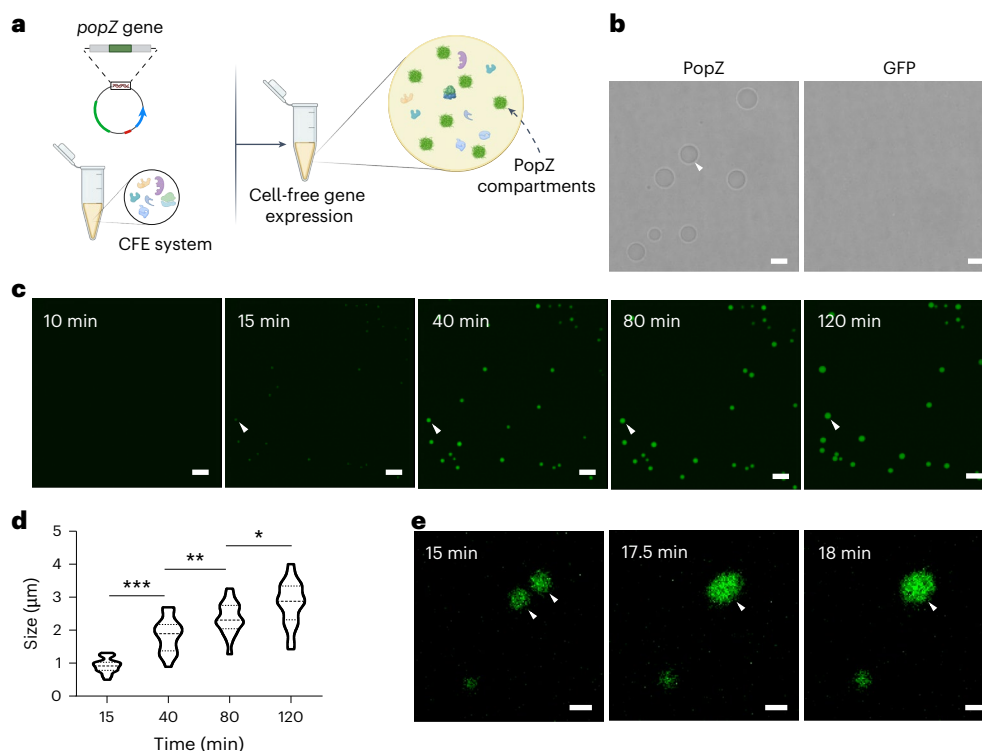
Fig. 1 | Formation of micron-sized PopZ compartments with liquid-like properties in CFE system. a, Schematics of de novo compartment formation through cell-free *popZ* gene expression. Created using BioRender.com. **b**, Confocal microscopy transmitted light images of the formed compartments (indicated by white arrowhead) in CFE of PopZ but not the GFP control. Both CFE reactions were incubated at 30 °C for 4 h. Scale bars, 5 μm. **c–e**, Time-lapse fluorescence imaging. For visualization of the CFE mixture, the *popZ* gene was spiked with its *gfpmut3* fusion at a molar ratio of 13.3:1. **c**, Monitoring of the evolving compartments under confocal microscope. Scale bars, 10 μm. **d**, Violin plots of the compartment size, with dashed and dotted lines indicating the median and interquartile values, respectively (*n* = 20). Statistical significance was determined using a one-way ANOVA (*P = 0.0248, **P = 0.0075 and ***P < 0.0001). **e**, Images showing fusion of two individual compartments. Scale bars, 1 μm. Data in **b–e** are representative of *n* = 2 independent experiments.

to condensation into the destination compartments in the CFE mixtures (Supplementary Fig. 7). Of particular interest, these preferences for charged fluorescent molecules were well retained when the two populations of compartments were coexisting (Extended Data Fig. 6). Further fluorescence recovery after photobleaching (FRAP) analysis revealed that the enriched fluorescent molecules were fairly mobile (Supplementary Fig. 8). This implied rapid exchange of the small molecules between the droplet-like compartments and the surrounding solution and inspired intercompartment delivery of these molecules.

Next, we designed two modes of small-molecule communication between the distinct compartments (Fig. 3a,b). In one scenario, we programmed the preformed PopZ compartments to send a small-molecule signal to the R32 compartments (Fig. 3a). The PopZ compartments were engineered to form and uptake SRh B in the CFE system first, followed by the emergence of the R32 compartments that grabbed SRh B from the surrounding solution and the PopZ compartments. This directional delivery of SRh B was spontaneous and driven by its repartitioning into the emerging R32 compartments. In particular, the ultimate SRh B fluorescence intensity in the PopZ compartments was reduced to the minimal level (Supplementary Fig. 9a), indicating almost complete delivery of the cargo to the destination (Fig. 3c). This observation may be explained by the greatly preferential partitioning of the small molecule within the compartment consortia in the pseudo-steady state (Extended Data Fig. 6b). In another scenario, we programmed the preformed R32 compartments to deliver another small molecule to the PopZ compartments (Fig. 3b). To this end, the R32 compartments were engineered to form and uptake Rh 6G and pyranine in the CFE system first, followed by the emergence of the PopZ compartments that selectively absorbed Rh 6G from the surrounding solution and

the preceding R32 compartments (Supplementary Fig. 9b). Despite incomplete delivery, the Rh 6G signal in the donor compartments was decreased by ~33% and the cargo concentration in the destination compartments was 2.7-fold higher than that of the donor (Fig. 3d). Overall, these results suggested that the synthetic compartment consortia can be programmed for bidirectional delivery of small-molecule cargoes and inspire further efforts to explore metabolite transport between coordinating compartments within living cells.

Programmable protein signaling between distinct compartments

Cells require highly specific and dynamic responses to process signals from the external environment and the information flow by signaling proteins through compartments in both space and time has a key role[27,28]. Given that protein–protein interactions are essential for their localization to specific subcellular organelles[27,28], we surmise that protein cargos could also be delivered from one compartment to another by altering the protein's affinity to them. To the best of our knowledge, such directional biomolecular communication has yet to be achieved in DNA-encoded biosynthetic systems. Therefore, we sought to achieve spatiotemporal communication of protein signal between distinct compartments in CFE systems. To this end, we selected a positively charged variant of GFP (GFP[15+])[29,30] as the cargo for delivery to the PopZ compartments. We installed a targeting sequence (His-tag), flexible linker and a cleavage site of tobacco etch virus protease (TEVp) at the N terminus of GFP[15+] (Fig. 4a). The resulting cargo precursor could be initially localized into the R32 compartments through His-tag-assisted heterotypic interactions and removal of the targeting sequence by TEVp would reduce affinity and allow the cargo to escape the R32 compartments for
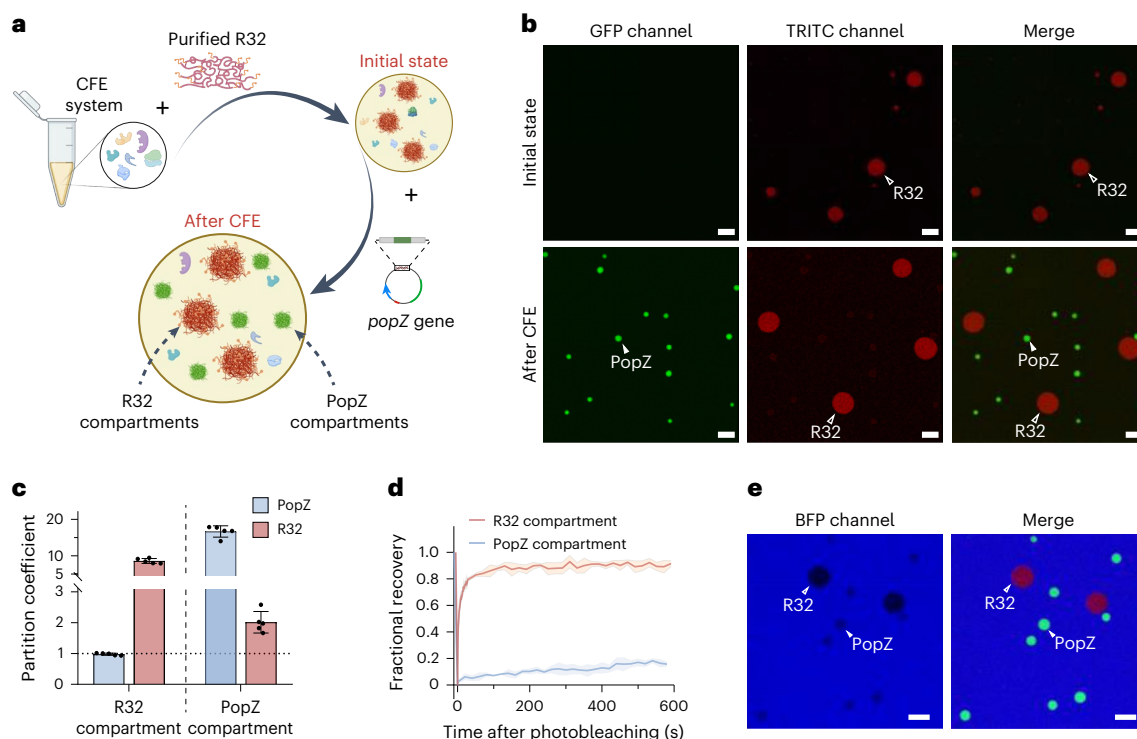
Fig. 2 | Construction of a binary population of orthogonal compartments.
a, Schematics of compartment consortium formation from exogenously added His–R32 and de novo expressed PopZ in the CFE system. Created using BioRender.com. **b**, Confocal fluorescence images of the mixture before and after CFE. The mixture contained His–R32 spiked with its TRITC conjugate at the molar ratio of 10:1 and the *popZ* gene spiked with its *gfpmut3* fusion at 13.3:1. Scale bars, 10 µm. **c**, Partition coefficient of proteins. Data are presented as the mean ± s.d. of $n = 5$ compartments, with individual data points shown as black dots. **d**, FRAP of the two populations of compartments. Data are presented as the mean ± s.d. of $n = 3$ compartments. **e**, Confocal images of the compartment consortia in the CFE mixture, within which 5 nM of the DNA template encoding BFP was supplemented. Scale bars, 5 µm. All the CFE systems containing 5 mM Ni^{2+} were incubated at 30 °C for 4 h. Data in **b–e** are representative of $n = 3$ independent experiments.

entering into the destination PopZ compartments. To test the design, we first verified that the targeting sequence of the precursor cargo was crucial for its localization into the R32 compartments (Extended Data Fig. 7a). In addition, the GFP[15+] cargo was favorably localized into the PopZ compartments, regardless of the presence of the initial targeting sequence (Extended Data Fig. 7b,c).

Next, we designed two modes of programmable protein cargo delivery between the distinct R32 and PopZ compartments. In the first scenario, the two compartments were engineered to form and then directed to execute the delivery task in response to an external TEVp signal (Fig. 4b). Intriguingly, the cargo precursor mostly accumulated in the 'sender' R32 compartments initially and the His-tagged protease signal triggered processing of the precursor into the ultimate cargo for release into the surrounding solution and delivery to the 'receiver' PopZ compartments. The kinetics of the intercompartment protein delivery was rather fast, which occurred within minutes (Extended Data Fig. 8) and appeared to be governed by the enzyme kinetics within the sender compartments involving cleavage of the targeting sequence by TEVp. In the second scenario, the preformed senders were allowed to process the enriched cargo precursor and deliver the cargo to the merging receivers. Again, directional delivery of the GFP[15+] cargo could be realized, indicating that processing of the cargo precursor in the pre-existing compartments was compatible with de novo formation of the receivers and their cargo adsorption (Fig. 4c). Quantitative analysis revealed that similar outcomes of intercompartment communication were achieved in the above two scenarios (Fig. 4d). These results supported that the compartment consortia can coordinate their processing and protein delivery tasks in a triggered and spatiotemporal manner and mimic the natural protein signaling for information flow through cascaded compartments in cells.

Intercompartment protein communication with feedback loops

In addition to spatiotemporal signaling, modulating the production of protein signals at the translation level is a fundamental and widely used strategy to control signal transduction pathways. This inspired us to explore whether feedback loop could be installed for regulating intercompartment protein communication at the mRNA level. To create a feedback loop in compartment consortia, we initially sought to assign the two populations of compartments as signal 'controller' and receiver. The controllers are functionalized with RNA-binding capability to sequester mRNA and reduce its translation into the client protein, thus attenuating the captured client in the receivers by establishing a negative feedback loop (Fig. 5a). Recent studies have shown that the RNA-binding domains (RBDs) are rich in RGG sequences and interact with the benzene rings in mRNA through cation–π interactions, thereby sequestering mRNA inside compartmentalized structures[31–33]. Thus, we made a PopZ fusion protein C-terminally tagged with RBD and found that its ability to form compartments was retained, whereas RBD alone did not phase-separate in the CFE system (Supplementary Fig. 10). As expected, the RBD-functionalized PopZ compartments attenuated expression of a model reporter protein (Supplementary Fig. 11) and cargo localization to the destination compartments (Extended Data Fig. 9). This indicates functioning of a negative feedback loop that 'puts the brakes' on the material flow from DNA to the protein and to the physical destination. We also found that the effectiveness of such negative feedback loops was tunable by adjusting the RBD functionalization degree of the controller PopZ compartments (Fig. 5b).

Lastly, we programmed intercompartment communication with negative feedback loops in response to DNA message triggers (Fig. 5c). The synthetic compartment consortium was composed of two
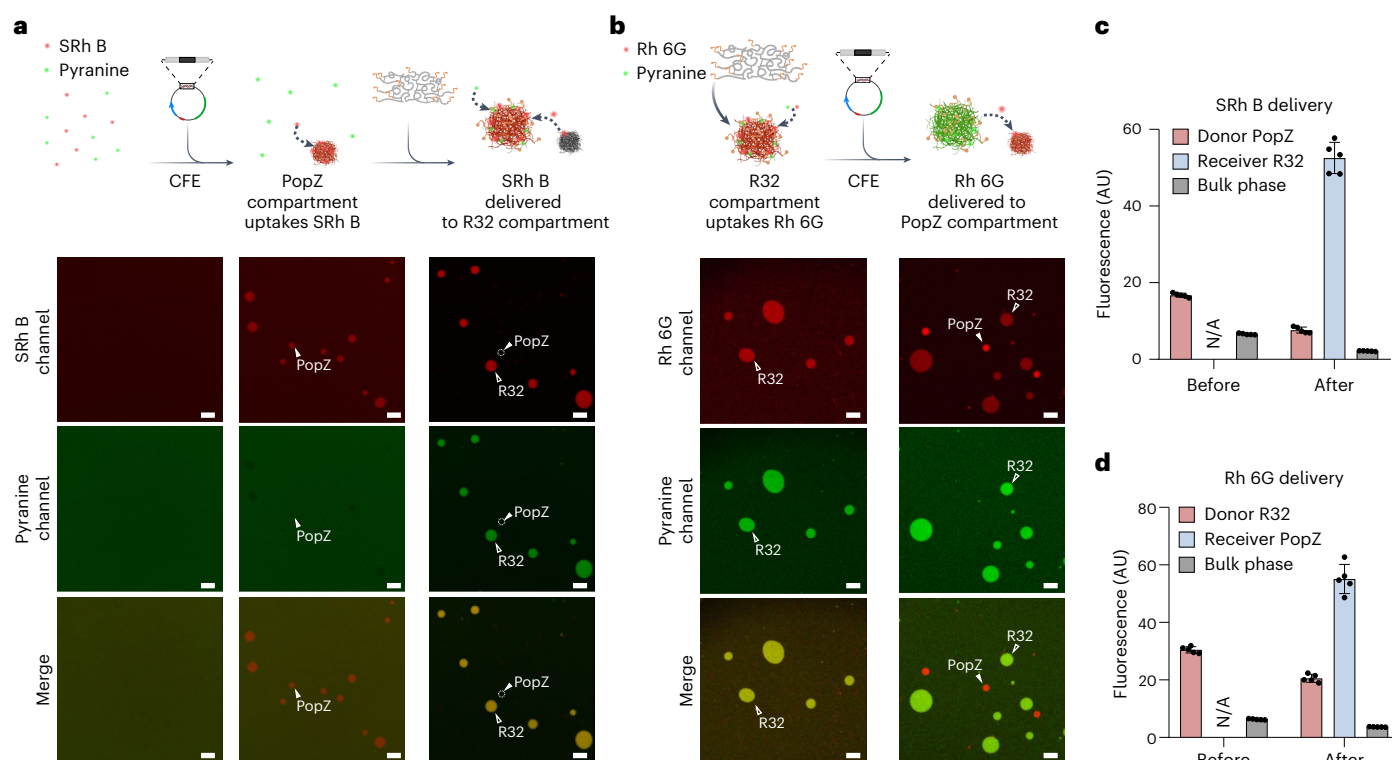
Fig. 3 | Programmable delivery of small molecules between orthogonal compartments. a, Schematics and confocal images of SRh B transport from the preformed PopZ compartments to the R32 compartments in the CFE system. The concentrations of fluorescent SRh B and pyranine were 50 and 200 µM, respectively. Scale bars, 10 µm. **b**, Schematics and confocal images of Rh 6G transport from the pre-existing R32 compartments to the PopZ compartments. The concentrations of fluorescent Rh 6G and pyranine were 50 and 200 µM, respectively. Scale bars, 10 µm. The appearance of the two populations of compartments was programmed by sequential addition of the *popZ* gene template (10.55 nM) and the purified His–R32 protein (10 mg ml⁻¹). The initial CFE mixtures were also supplemented with 5 mM Ni²⁺, incubated at 30 °C for 4 h for PopZ expression and imaged. The schematics in **a,b** were created using BioRender.com. **c,d**, Fluorescence intensity (arbitrary units (AU)) of the donor and receiver compartments and the surrounding bulk phase before and after SRh B delivery (**c**) and Rh 6G delivery (**d**). Data are presented as the mean ± s.d. of $n = 5$ compartments or regions of bulk phase. N/A, not applicable, because of the absence of the receiver compartments at the moment. Data in **a–d** are representative of $n = 3$ independent experiments.

populations of compartments: one classified as a depot and processer and the other classified as a controller and receiver. First, biogenesis of the precursor cargo protein from its DNA was programmed to occur for prior localization into the depot R32 compartments in the CFE system (Fig. 5d). Two DNA inputs were then implemented; one input yielded His–TEVp to be targeted into the depot within which the precursor cargo was processed into the cargo GFP¹⁵⁺ for release and the other input yielded the PopZ–RBD protein to form compartments that captured the released cargo. In addition, the RBD-functionalized PopZ compartments could sequester the transcribed mRNA molecules and, thus, negatively control the information flow of the two DNA inputs. Fluorescence imaging of the compartment consortia revealed tunable outcomes of the intercompartment cargo communication in time and space (Extended Data Fig. 10). As typically demonstrated at 4 h after communication (Fig. 5e–g), elevating the functionalization degree of the controller compartments led to a moderate increase in the remaining cargo precursor in the depot, which was attributed to incomplete enzymatic cleavage resulting from reduced biogenesis and recruitment of the TEVp. This attenuated formation of the cargo and its release into the surrounding solution contributed to the marked decrease in the cargo captured within the PopZ compartments (Fig. 5h). Together, these results proved that the intercompartment protein signaling could be programmed to be responsive to DNA-based messages in a tunable manner.

Discussion

Our study demonstrates programmable formation and biological communication between two distinct populations of membraneless compartments under cellular environmental conditions. The compartment consortia are unique in that they are physically separated, compositionally and functionally independent yet smoothly coordinated to perform complex biological tasks. These features largely recapitulate the fascinating feats of living cells by structural organization of cellular and metabolic activities in diverse MLOs. Despite being constructed in cell-free extracts and lipid-enclosed protocells, the synthetic compartment consortia may inspire endeavors to transplant them into living cells for modulation of metabolic and cellular behaviors³⁴,³⁵.

To better mimic the cellular environment for compartment consortium formation and functioning, we made modifications to the classical CFE system. First, we removed the macromolecular crowding agent polyethylene glycol because this chemical polymer is not a naturally occurring biological component and may potentially cause abnormal increases in the recruitment of substances into compartments³⁶,³⁷. Second, we appropriately increased the glutamate salt concentration and added a small amount of the nickel ion (5 mM) in the CFE mixtures. In particular, the nickel ion had critical roles: expedition (Supplementary Fig. 5) and stabilization (Supplementary Fig. 12) of the formation of a compartment population derived from His–R32 and enrichment of both His–TEVp and cargo protein into the resultant R32 compartments such that spatiotemporal removal of the cargo targeting sequence occurs for subsequent intercompartment delivery. Moreover, the nickel ion can influence the size of the emerging PopZ compartment in the CFE systems (Supplementary Fig. 13). It is also worth noting that the compartment formation by phase separation is closely linked to the protein identities, their expression rates in cells and the surrounding
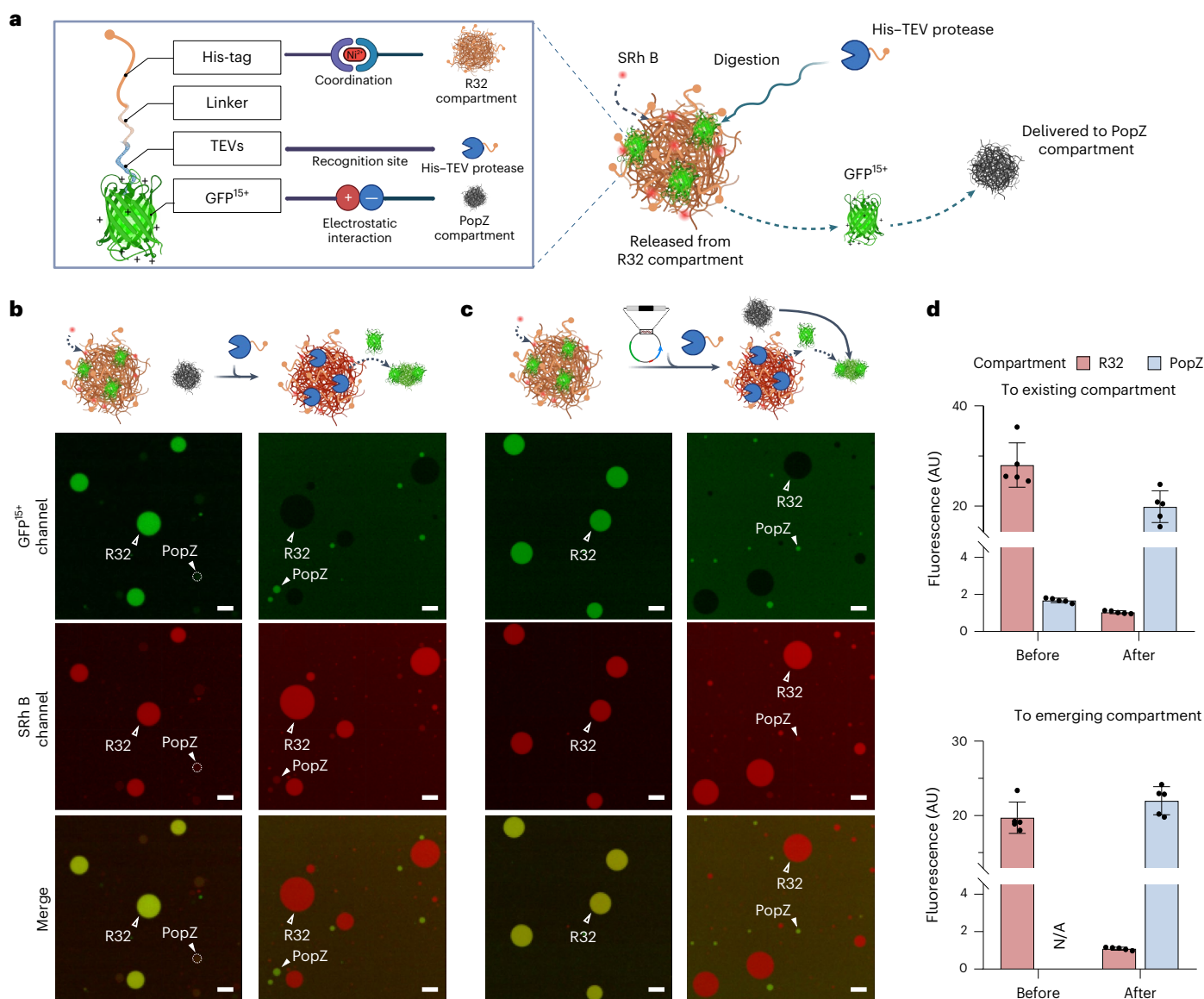
Fig. 4 | Protein signaling between distinct compartments. a, Design of a precursor protein cargo GFP[15+] by installing a His-tag and TEVs. These two motifs enable the precursor to be enriched and processed in the R32 compartments for cargo release and delivery to the PopZ compartments. **b**,**c**, Schematic drawing and confocal images of cargo delivery from the R32 compartments to the existing (**b**) or merging (**c**) PopZ compartments. CFE of the precursor protein was conducted at 30 °C for 2 h in the mixtures containing 10 mg ml⁻¹ His–R32, 5 mM Ni²⁺ and 5 µM SRh B, followed by 4-h expression of the *popZ* gene to form the coexisting PopZ compartments before the addition of 8.82 µM TEVp for 2-h

treatment. Alternatively, the *popZ* gene and TEVp were added simultaneously for triggering cargo delivery to the emerging PopZ compartments. Scale bars, 10 µm. The schematics in **a**–**c** were created in BioRender.com. **d**, Fluorescence intensity (AU) of GFP[15+] in the R32 and PopZ compartments before and after the protease-triggered cargo delivery. Shown are the two modes of signaling from the R32 compartments to the existing (top) or emerging PopZ compartments (bottom). Data are presented as the mean ± s.d. of $n = 5$ compartments. N/A, because of the absence of the PopZ compartments at the moment. Data in **b**–**d** are representative of $n = 3$ independent experiments.

environment[21,38–40]. The inherent advantages of CFE system allow us to adjust key components in the reactions, such as DNA template concentrations affecting protein expression rates. Through these means, we allowed the CFE system to be highly compatible with compartment consortium formation, maintenance of their structural stability and dynamic properties and on-demand recruitment and release of small molecules and protein cargoes for localization into specific compartments. The design principles established herein will be particularly helpful for the synthetic design and construction of coordinating compartment consortia with programmable on-demand functions and dynamics.

So far, communication between natural MLOs is underexplored[7] and our understanding of inter-MLO crosstalk and the underlying

mechanisms remains limited[6,41]. For example, a rheostat-like mechanistic paradigm is proposed for regulating live-or-die cell-fate decisions in macrophages under stress conditions, under which stress granules and the NLRP3 inflammasomes compete for the stress granule protein DDX3X to coordinate the activation of innate responses[6]. Increasing evidence has suggested that MLOs often share macromolecular components that are likely to communicate with each other[6,7,41,42] and protein signals have an important role for the inter-MLO communication in cells. This feature is well emulated in our artificial design and construction. We showed that cleavage of the targeting peptide from the precursor cargo could spatiotemporally occur to reduce its interaction with the 'depot' compartment components for release and repartitioning into the receiver compartment and feedback loops could be
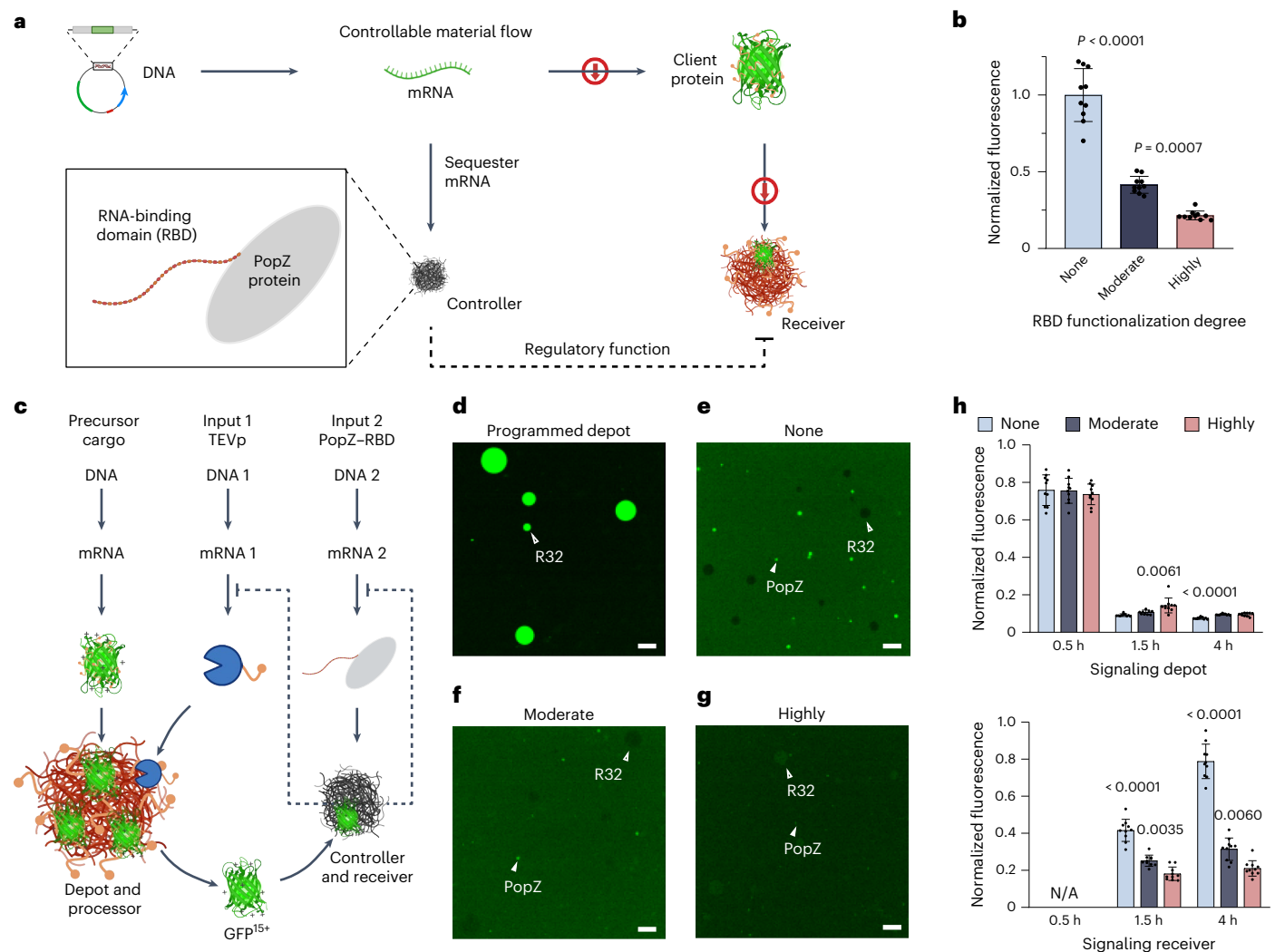
Fig. 5 | Intercompartment communication with negative feedback loops.
a, Establishing a negative feedback loop. The controller compartment was functionalized to sequester mRNA and decrease client protein translation and localization to the receiver compartment. **b**, Relative fluorescence of client in the receiver R32 compartments by varying functionalization degree of the controller compartment with RNA-binding capability. The CFE systems also contained a client template (4.90 nM) encoding histidine-tagged GFPmut3, 10 mg ml^{-1} His−R32 protein and 5 mM Ni^{2+}. **c**, Programmable intercompartment protein delivery with negative feedback. **d**, Image of the depot R32 compartments programmed to enrich a targeting sequence-tagged GFP^{15+}. This precursor cargo was synthesized from the *His−TEVs−gfp^{15+}* gene by CFE at 30 °C for 2 h

in the initial mixtures that also contained 10 mg ml^{-1} His−R32 and 5 mM Ni^{2+}. **e**−**g**, Images of the R32 compartments and the emerging PopZ compartments with varying RBD functionalization degrees: none (**e**), moderate (**f**) and highly (**g**). The necessary *popZ* templates and 2.03 nM *His−TEVp* gene were added as DNA triggers into the CFE systems for additional 4-h incubation. For clarity, the brightness and contrast of the images in **d**−**g** were adjusted. Scale bars, 10 µm. **h**, Relative fluorescence of GFP^{15+} in the depot and receiver compartments. N/A, because of the absence of the PopZ compartments at the moment. Data in **b**,**h** are presented as the mean ± s.d. of *n* = 10 compartments and one-way ANOVA was used to determine the *P* values shown. The schematics in **a**,**c** were created using BioRender.com.

installed to tune the degrees of the protein crosstalk. This suggested a molecular mechanism through protease-triggered modulation of cargo affinities for different compartment components. Furthermore, the synthetic compartment consortia developed here expand the known communication capability to bidirectional delivery of small molecules, which raises questions on whether such a molecular mechanism may operate in intracellular MLO crosstalk and the tentative physiological or pathological outcomes.

Online content

Any methods, additional references, Nature Portfolio reporting summaries, source data, extended data, supplementary information, acknowledgements, peer review information; details of author contributions and competing interests; and statements of data and code availability are available at https://doi.org/10.1038/s41589-025-01840-4.

References

1. Bar-Peled, L. & Kory, N. Principles and functions of metabolic compartmentalization. *Nat. Metab.* **4**, 1232–1244 (2022).
2. Zhao, Y. G. & Zhang, H. Phase separation in membrane biology: the interplay between membrane-bound organelles and membraneless condensates. *Dev. Cell* **55**, 30–44 (2020).
3. Lyon, A. S., Peeples, W. B. & Rosen, M. K. A framework for understanding the functions of biomolecular condensates across scales. *Nat. Rev. Mol. Cell Biol.* **22**, 215–235 (2021).
4. Shin, Y. & Brangwynne, C. P. Liquid phase condensation in cell physiology and disease. *Science* **357**, eaaf4382 (2017).
5. Villegas, J. A., Heidenreich, M. & Levy, E. D. Molecular and environmental determinants of biomolecular condensate formation. *Nat. Chem. Biol.* **18**, 1319–1329 (2022).

6. Samir, P. et al. DDX3X acts as a live-or-die checkpoint in stressed cells by regulating NLRP3 inflammasome. *Nature* **573**, 590–594 (2019).

7. Hirose, T., Ninomiya, K., Nakagawa, S. & Yamazaki, T. A guide to membraneless organelles and their various roles in gene regulation. *Nat. Rev. Mol. Cell Biol.* **24**, 288–304 (2023).

8. Welles, R. M. et al. Determinants that enable disordered protein assembly into discrete condensed phases. *Nat. Chem.* **16**, 1062–1072 (2024).

9. Ye, S. et al. Micropolarity governs the structural organization of biomolecular condensates. *Nat. Chem. Biol.* **20**, 443–451 (2024).

10. Choi, S., Meyer, M. O., Bevilacqua, P. C. & Keating, C. D. Phase-specific RNA accumulation and duplex thermodynamics in multiphase coacervate models for membraneless organelles. *Nat. Chem.* **14**, 1110–1117 (2022).

11. Mu, W. et al. Superstructural ordering in self-sorting coacervate-based protocell networks. *Nat. Chem.* **16**, 158–167 (2024).

12. Qi, C. et al. Multicompartmental coacervate-based protocell by spontaneous droplet evaporation. *Nat. Commun.* **15**, 1107 (2024).

13. Kaur, T. et al. Sequence-encoded and composition-dependent protein–RNA interactions control multiphasic condensate morphologies. *Nat. Commun.* **12**, 872 (2021).

14. Zhao, Q. H., Cao, F. H., Luo, Z. H., Huck, W. T. S. & Deng, N. N. Photoswitchable molecular communication between programmable DNA-based artificial membraneless organelles. *Angew. Chem. Int. Ed. Engl.* **61**, e202117500 (2022).

15. Mashima, T. et al. DNA-mediated protein shuttling between coacervate-based artificial cells. *Angew. Chem. Int. Ed. Engl.* **61**, e202115041 (2022).

16. van Veldhuisen, T. W., Verwiel, M. A. M., Novosedlik, S., Brunsveld, L. & van Hest, J. C. M. Competitive protein recruitment in artificial cells. *Commun. Chem.* **7**, 148 (2024).

17. Silverman, A. D., Karim, A. S. & Jewett, M. C. Cell-free gene expression: an expanded repertoire of applications. *Nat. Rev. Genet.* **21**, 151–170 (2020).

18. Garenne, D. & Noireaux, V. Cell-free transcription–translation: engineering biology from the nanometer to the millimeter scale. *Curr. Opin. Biotechnol.* **58**, 19–27 (2019).

19. Holmes, J. A. et al. *Caulobacter* PopZ forms an intrinsically disordered hub in organizing bacterial cell poles. *Proc. Natl Acad. Sci. USA* **113**, 12490–12495 (2016).

20. Lasker, K. et al. Selective sequestration of signalling proteins in a membraneless organelle reinforces the spatial regulation of asymmetry in *Caulobacter crescentus*. *Nat. Microbiol.* **5**, 418–429 (2020).

21. Wei, S. P. et al. Formation and functionalization of membraneless compartments in *Escherichia coli*. *Nat. Chem. Biol.* **16**, 1143–1148 (2020).

22. Farag, M., Borcherds, W. M., Bremer, A., Mittag, T. & Pappu, R. V. Phase separation of protein mixtures is driven by the interplay of homotypic and heterotypic interactions. *Nat. Commun.* **14**, 5527 (2023).

23. Ebersbach, G., Briegel, A., Jensen, G. J. & Jacobs-Wagner, C. A self-associating protein critical for chromosome attachment, division, and polar organization in *Caulobacter*. *Cell* **134**, 956–968 (2008).

24. Bowman, G. R. et al. A polymeric protein anchors the chromosomal origin/ParB complex at a bacterial cell pole. *Cell* **134**, 945–955 (2008).

25. Lasker, K. et al. The material properties of a bacterial-derived biomolecular condensate tune biological function in natural and synthetic systems. *Nat. Commun.* **13**, 5643 (2022).

26. Dzuricky, M., Rogers, B. A., Shahid, A., Cremer, P. S. & Chilkoti, A. De novo engineering of intracellular condensates using artificial disordered proteins. *Nat. Chem.* **12**, 814–825 (2020).

27. Kedersha, N. et al. Stress granules and processing bodies are dynamically linked sites of mRNP remodeling. *J. Cell Biol.* **169**, 871–884 (2005).

28. Courchaine, E. M. et al. DMA–tudor interaction modules control the specificity of *in vivo* condensates. *Cell* **184**, 3612–3625 (2021).

29. McNaughton, B. R., Cronican, J. J., Thompson, D. B. & Liu, D. R. Mammalian cell penetration, siRNA transfection, and DNA transfection by supercharged proteins. *Proc. Natl Acad. Sci. USA* **106**, 6111–6116 (2009).

30. Thompson, D. B., Villaseñor, R., Dorr, B. M., Zerial, M. & Liu, D. R. Cellular uptake mechanisms and endosomal trafficking of supercharged proteins. *Chem. Biol.* **19**, 831–843 (2012).

31. Chong, P. A., Vernon, R. M. & Forman-Kay, J. D. RGG/RG motif regions in RNA binding and phase separation. *J. Mol. Biol.* **430**, 4650–4665 (2018).

32. Simon, J. R., Eghtesadi, S. A., Dzuricky, M., You, L. & Chilkoti, A. Engineered ribonucleoprotein granules inhibit translation in protocells. *Mol. Cell* **75**, 66–75 (2019).

33. Robinson, A. O., Lee, J., Cameron, A., Keating, C. D. & Adamala, K. P. Cell-free expressed membraneless organelles inhibit translation in synthetic cells. *ACS Biomater. Sci. Eng.* **10**, 773–781 (2024).

34. Dai, Y., You, L. & Chilkoti, A. Engineering synthetic biomolecular condensates. *Nat. Rev. Bioeng.* **1**, 466–480 (2023).

35. Qian, Z. G., Huang, S. C. & Xia, X. X. Synthetic protein condensates for cellular and metabolic engineering. *Nat. Chem. Biol.* **18**, 1330–1340 (2022).

36. Jo, Y., Jang, J., Song, D., Park, H. & Jung, Y. Determinants for intrinsically disordered protein recruitment into phase-separated protein condensates. *Chem. Sci.* **13**, 522–530 (2022).

37. Kato, S., Garenne, D., Noireaux, V. & Maeda, Y. T. Phase separation and protein partitioning in compartmentalized cell-free expression reactions. *Biomacromolecules* **22**, 3451–3459 (2021).

38. Quiroz, F. G. & Chilkoti, A. Sequence heuristics to encode phase behaviour in intrinsically disordered protein polymers. *Nat. Mater.* **14**, 1164–1171 (2015).

39. Dai, Y. et al. Programmable synthetic biomolecular condensates for cellular control. *Nat. Chem. Biol.* **19**, 518–528 (2023).

40. Pan, F., Zu, H., Zhu, Y. J., Qian, Z. G. & Xia, X. X. Spatiotemporal organization of functional cargoes by light-switchable condensation in *Escherichia coli* cells. *JACS Au* **4**, 1480–1488 (2024).

41. Sanders, D. W. et al. Competing protein–RNA interaction networks control multiphase intracellular organization. *Cell* **181**, 306–324 (2020).

42. Zhu, S. et al. Demixing is a default process for biological condensates formed via phase separation. *Science* **384**, 920–928 (2024).

Methods

Bacterial strains and plasmids

E. coli strains DH5α and Top10 were routinely used as hosts for plasmid construction and propagation and *E. coli* BL21(DE3) was used for preparation of cell extract and small-scale preparation of recombinant proteins. The plasmids and oligonucleotide primers used in this study are listed in Supplementary Tables 1 and 2, respectively. DNA sequences encoding the codon-optimized PopZ[24], a mutant version of TEVp (Addgene, 193833), GFP[15+] (ref. [30]), RBD[31] and mTagBFP2 (ref. [43]) were purchased as synthetic genes from Genewiz. The amino acid sequences of these proteins and polypeptide domains can be found in Supplementary Table 3.

For CFE of proteins, a series of expression plasmids based on vector pJL1 (a gift from Y. Lu) were constructed. To construct plasmid pJL1-popZ for PopZ expression, the codon-optimized *popZ* gene was amplified from plasmid pET28a-popZ (Supplementary Table 1) by PCR using primers FpopZNde and RpopZSal from Genewiz (Supplementary Table 2), restricted with enzymes NdeI and SalI-HF and inserted into vector pJL1 at the same sites. For expression of PopZ N-terminally fused to GFPmut3 (ref. [44]), plasmid pJL1-popZGFP′ was made by amplifying the *popZ–gfp*′ fusion from plasmid pET28a4-popZGFP′ with primers FpopZgNde and RpopZgSal and then cloned into the NdeI and SalI sites of vector pJL1. To create plasmid pET28a4-popZGFP′, the *popZ* gene was first amplified from pET28a-popZ with PCR primers FpopZNde-1 and RpopZSpe, restricted with enzymes NdeI and SpeI-HF and inserted into pET28a4-I16-GFP′ (ref. [21]) at the same sites. For expression of PopZ C-terminally fused to GFPmut3, plasmid pJL1-GFP′popZ was made. The *gfpmut3* fragment was amplified from plasmid pJL1-popZGFP′ with primers FgfpNde and RgfpSpe and the *popZ* gene was amplified from pET28a-popZ with primers FpopZSpe and RpopZSal-1. The resulting PCR products were restricted with enzyme pair NdeI/SpeI-HF and SpeI-HF/SalI-HF, respectively, and then ligated with the 1.8-kb NdeI–SalI fragment of vector pJL1 to yield plasmid pJL1-GFP′popZ. For expression of GFPmut3 serving as a control, pJL1-GFP′ was constructed by Gibson assembly of the linearized vector (amplified from pJL1 with primers FpJL and RpJL) and the *gfpmut3* fragment, which was amplified from pET28a4-GFP′ (ref. [21]) with primers Fgfp and Rgfp. For expression of decahistidine-tagged GFPmut3, plasmid pJL1-His–GFP′ was constructed by amplifying the *gfpmut3* fragment from pJL1-popZGFP′ with primers FHisgNde and RHisgSal and cloned into the NdeI and SalI sites of vector pJL1.

For programmable protein delivery between compartments, a series of CFE plasmids were made. First, plasmid pJL1-His–TEVp was constructed for expression of decahistidine-tagged TEVp. The DNA fragment encoding TEVp was amplified from pACYCDuet-1-TEVp, which harbored the synthetic gene, with primers FHisTNde and RHisTSal, digested with NdeI and SalI-HF and inserted into vector pJL1 at the same sites to construct pJL1-His–TEVp. For expression of TEVp substrates containing the TEV recognition site (TEVs), plasmids pJL1-His6–TEV$_S$–GFP[15+] and pJL1-His–TEV$_S$–GFP[15+] were made, which encoded hexahistidine- and decahistidine-tagged TEVs–GFP[+15] fusions, respectively. To this end, plasmid pJL1-His6–TEV$_S$–GFP[15+] was first generated by Gibson assembly of the TEVs fragment (annealed with oligonucleotides FTEVs and RTEVs) and the vector backbone (amplified from pJL1-His6–GFP[15+] with primers FpJLg and RpJLg). Then, the DNA fragment encoding TEVs–gfp[15+] was amplified from plasmid pJL1-His6–TEVs–GFP[15+] using primers Flinker and Rg15Sal-1. This PCR product was used as the template for the second round of PCR using primers FHislNde and Rg15Sal-1 to add the decahistidine tag and a linker sequence upstream of TEVs–GFP[15+]. The resulting DNA fragment was subsequently digested with NdeI and SalI-HF and ligated with the 1.8-kb NdeI–SalI fragment of vector pJL1 to make construct pJL1-His–TEVs–GFP[15+]. For expression of control proteins not recognized by TEVp, plasmids pJL1-GFP[15+] and pJL1-His–GFP[15+] were constructed that encode untagged and decahistidine-tagged GFP[15+], respectively. Briefly, the fragment encoding GFP[15+] was amplified from

the template plasmid pJL1-His6–GFP[15+] (purchased from Genewiz) with primers Fg15 and Rg15Sal. This PCR product was used as the template for the second round of PCR with primers Fg15Nde and Rg15Sal. The resulting DNA was then restricted with NdeI and SalI-HF and cloned into vector pJL1 to make plasmid pJL1-GFP[15+]. In a similar manner, the plasmid pJL1-His–GFP[15+] was made except that primers FHisg15Nde and RHisg15Sal were used.

For mRNA sequestration into protein compartments, plasmid pJL1′-popZRBD encoding PopZ–RBD fusion protein was constructed. In PopZ–RBD, functionalization with RNA-binding capability was achieved by genetically fusing one copy of RBD to PopZ at the C terminus. To facilitate cloning, plasmid pJL1′ was derived from pJL1 by replacement of the SalI site on the vector backbone with BamHI site, using the KOD-Plus mutagenesis kit (SMK-101, TOYOBO) and primers FpJL′ and RpJL′. Then, the *popZ* and *RBD* fragments were liberated by NdeI/SpeI-HF digest of plasmid pJL1-popZGFP′ and SpeI-HF/BamHI-HF digest of plasmid pET28a4-R32RBD, respectively, and ligated with the 1.8-kb NdeI–BamHI fragment of vector pJL1′ to make plasmid pJL1′-popZRBD. In another setup, the *mTagBFP2* gene was amplified from plasmid pJL1-mTagBFP2 with primers FbfpSpe and RbfpBam and cloned into the SpeI–BamHI site of pJL1′-popZRBD to replace the RBD fragment. The resulting plasmid pJL1′-popZmTagBFP2 encoded a fusion PopZ–mTagBFP2 protein.

Biosynthesis of recombinant protein and fluorescent labeling

For small-scale preparation of recombinant proteins, *E. coli* BL21(DE3) cells carrying the intended expression plasmid were used for biosynthesis in shake flasks. Following purification, the protein concentrations were determined using the protein A_{280} method in combination with the protein's molar extinction coefficient. The A_{280} absorbance values were acquired on a NANO DROP 2000 spectrophotometer (Thermo Fisher Scientific).

E. coli BL21(DE3) cells carrying plasmid pET19b-R32 (ref. [45]) were used for the production of resilin-like protein R32 as described previously[45]. The harvested cells were suspended in 20 mM Tris-HCl buffer pH 8.0 containing 150 mM NaCl and 5 mM imidazole and then lysed using a high-pressure homogenizer. The target R32 protein was subsequently purified from the cell lysate using immobilized metal affinity chromatography (IMAC), extensively dialyzed against deionized water and lyophilized. Before fluorescent labeling, the lyophilized protein was dissolved in 20 mM HEPES–KOH buffer pH 8.2 to a concentration of 6 mg ml^{-1}, with the addition of TRITC (T131567, Aladdin) to a final concentration of 35 μg ml^{-1}. The mixture was then incubated at room temperature in the darkness for 2 h and the unconjugated TRITC in the mixture was removed using a desalting column (28918007, Cytiva). The resulting solution of the fluorescently labeled protein was concentrated to ~50 mg ml^{-1} using an Amicon Ultra-0.5 centrifugal device with a filter with a 10-kDa molecular weight cutoff (UFC5010BK, Millipore).

E. coli BL21(DE3) harboring plasmid pET28a4-GFP′ was used for small-scale preparation of the hexahistidine-tagged GFPmut3 by flask cultivation. The recombinant protein was then purified from the cell lysate using IMAC, dialyzed against 50 mM HEPES–KOH buffer pH 7.5 and used as a fluorescent protein standard.

Preparation of cell extract

E. coli BL21(DE3) cells were grown in a 2-L baffled flask containing 1 L of 2× YTPG medium at 37 °C and 220 rpm in a shaking incubator. The 2× YTPG medium contained 10 g L^{-1} yeast extract, 16 g L^{-1} tryptone, 5 g L^{-1} NaCl, 7 g L^{-1} K$_2$HPO$_4$, 3 g L^{-1} KH$_2$PO$_4$ and 18 g L^{-1} glucose. When the cell optical density at 600 nm (OD$_{600}$) reached 0.6–0.8, IPTG was added at a final concentration of 1 mM to induce the expression of chromosome-encoded T7 RNA polymerase. When the OD$_{600}$ of the induced cells reached 3.0–4.0, the cells were harvested by centrifugation. The cells were washed three times with prechilled S30 buffer (10 mM Tris, 14 mM magnesium glutamate and 60 mM potassium

glutamate; pH adjusted to 8.2 with acetic acid) containing 2 mM DTT. The cells were then resuspended in the fresh S30 buffer (1 ml per 1 g of fresh cells) and disrupted by a high-pressure homogenizer. Following the supplementation of additional 2 mM DTT, the cell lysates were centrifuged at 18,000g for 10 min at 4 °C to collect the supernatant, which was incubated at 37 °C and 220 rpm for 60 min to complete the runoff reaction. After centrifugation at 12,000g for 10 min at 4 °C, the supernatant was collected as the cell extract, which was fluorescently labeled or snap-frozen in liquid nitrogen and stored at −80 °C until use.

Fluorescent labeling of cell extract
The cellular extract was dialyzed at 4 °C overnight against 20 mM HEPES−KOH buffer pH 7.5 using a dialysis tubing with 3.5-kDa molecular weight cutoff (20530ES03, Yeasen Biotechnology). Then, 5(6)-FAM (BD130603, Bidepharm) was added to a final concentration of 1 μM and the mixture was incubated on ice for 2 h to label the cellular proteins in the cell extract. The unconjugated 5(6)-FAM was then removed using a desalting column and the labeled cell extract was stored on ice for further use.

Construction of CFE system
Cell-free gene expression was performed at 30 °C in a volume of 15 μl in 1.5-ml Eppendorf tubes. The standard reaction mixture consisted of 57 mM HEPES−KOH pH 7.5, 1.2 mM adenosine triphosphate and 0.85 mM each of guanosine triphosphate, uridine triphosphate and cytidine triphosphate, 34.0 μg ml^{-1} leucovorin; 170.0 μg ml^{-1} $E. coli$ transfer RNA mixtures, 180 mM potassium glutamate, 10 mM ammonium glutamate, 10 mM magnesium glutamate, 2 mM each of the 20 canonical amino acids, 0.33 mM nicotinamide adenine dinucleotide, 0.27 mM coenzyme A, 1.5 mM spermidine, 1 mM putrescine, 2.7 mM sodium oxalate, 33 mM phosphoenolpyruvate and 33% v/v of cell extract. For exploration of the distribution of cellular proteins in the reaction mixtures, 7% v/v of the fluorescently labeled cell extract was additionally added. DNA template was added at the indicated concentration for triggering production of the protein of interest and no DNA reaction mixture was prepared and incubated as a control.

For monitoring of the CFE, the reaction mixtures were diluted twofold with 50 mM HEPES−KOH buffer pH 7.5 and transferred to a covered 384-well plate in a Spark multimode microplate reader (Tecan). Fluorescence intensities were then recorded and concentrations of the proteins synthesized in the cell-free reactions were calculated according to a standard curve generated from the purified GFPmut3 protein using the software Origin 2017 (OriginLab Corporation).

Construction of compartment consortia
Typically, compartment consortia were prepared by adding the purified R32 protein to the CFE system at 10 mg ml^{-1}, which spontaneously phase-separated into compartments. In addition, 5 mM NiCl$_2$ was added for stabilization of the R32 protein compartments in the cell-free reactions. The CFE mixtures containing the $popZ$-encoding templates were incubated at 30 °C to allow de novo biosynthesis of PopZ to form coexisting compartments. For probing the distinct populations of compartments, fluorescent small molecules SRh B, Rh 6G and pyranine were included in the CFE mixtures at specified concentrations in the range of 5−200 μM. The partition coefficient of each molecule was calculated by dividing the intensity of fluorescent signal in the droplet region discernable as protein compartments by the intensity of the bulk environment, using software Microsoft Excel 2021 (Microsoft Corporation). Notably, the reconstituted mixtures had salt concentrations mimicking the cytoplasmic physiological conditions of cells[18], with pH homeostasis well maintained over extended time of CFE incubation (Supplementary Fig. 14).

Intercompartment delivery of protein cargo
DNA template encoding the cargo protein His−TEVs−GFP[15+] was added at 4.77 nM to the CFE system, along with 10 mg ml^{-1} R32 and 5 mM

NiCl$_2$. The resulting mixture (15 μl), which contained the R32 protein compartments, was incubated at 30 °C for 2 h. Then, 2 μL each of the PopZ-encoding plasmid and recombinant His−TEVp (P2307, Beyotime Biotechnology) were added into the CFE mixture either simultaneously or in a sequential manner. Upon simultaneous addition of the plasmid template and protease, the reaction was conducted at 30 °C for 6 h. Alternatively, the reaction mixture was added with the $popZ$ template to synthesize PopZ for 4 h and then the His−TEVp was mixed and incubated for additional 2 h.

Program protein cargo delivery between distinct compartments
For characterization of the RBD-functionalized PopZ compartments, DNA templates encoding the PopZ−RBD fusion and His−GFP were simultaneously added to the cell-free system at 10.55 and 4.90 nM, respectively. In addition, 10 mg ml^{-1} R32 and 5 mM NiCl$_2$ were included in the reaction mixture for incubation at 30 °C for 4 h. A control reaction mixture was also prepared by replacing the $popZ−RBD$ template with the unfunctionalized $popZ$ template. In another setup, the $popZ$ gene and $popZ−RBD$ fusion gene was added at a molar ratio of 1:1. The fluorescent intensities of His−GFP in the receiver R32 compartments were then determined for the above three reaction mixtures.

To construct a gene circuit for negative feedback regulation of cargo delivery, the DNA template encoding His−TEVs−GFP[15+] (9.54 nM), purified R32 (10 mg ml^{-1}) and NiCl$_2$ (5 mM) were added to the cell-free system for incubation at 30 °C for 2 h. The controller compartments with varied RBD functionalization degrees emerged from CFE of the $popZ$ gene (none), $popZ−RBD$ fusion gene (highly) or their 1:1 mixture (moderate) at 8.79 nM. The DNA template encoding His−TEVp was added at 2.03 nM for additional incubation up to 4 h. The reaction mixtures were sampled periodically and imaged under the confocal microscope.

Confocal imaging
The confocal images were collected on a Leica TCS SP8 STED 3 microscope (Leica Microsystems). The specimens were illuminated with a 405-nm, 488-nm and 561-nm laser for blue, green and red fluorescence imaging and with a 633-nm laser for bright-field imaging. All images were acquired with the Leica LAS X software version 3.7.1.21655 (Leica Microsystems) and analyzed using ImageJ version 1.53e, a freely available image-processing program (https://imagej.net/ij/).

FRAP
FRAP was performed using the Leica TCS SP8 STED ×3 microscope with a 65-mW Ar laser exciting at 488 nm or a 20 mW diode-pumped solid-state laser exciting at 561 nm. Bleaching was performed at 100% laser power (488 nm) or 80% laser power (561 nm). Following bleaching, images were captured every second for 20−30 s to record fluorescence recovery. The intensities of the region of bleaching (ROB), background region (BG) and reference region (REF) were measured using the Leica LAS X software. Subsequently, the fluorescence intensities were background-corrected and normalized according to the protocol reported by Hong et al.[46] $(I_{ROB} − I_{BG})/(I_{REF} − I_{BG})$ before photobleaching was set to 1 and $(I_{ROB} − I_{BG})/(I_{REF} − I_{BG})$ right after photobleaching was set to 0. Recovery curves were then generated by plotting $(I_{ROB} − I_{BG})/(I_{REF} − I_{BG})$ against time.

Sealed slide chamber for continuous observation
The glass slides were soaked in 5% BSA overnight to hydrophobize their surfaces, rinsed with deionized water and then dried until use. After pasting the slide chamber (SLF0201, Bio-Rad) on one slide, the CFE mixture was dropped in the center of the slide and then sealed by another glass slide. The prepared sealed slide chamber was subsequently placed in a heating device on the microscope stage to maintain a temperature of 30 °C. Confocal images were taken every 5 min.

Preparation of synthetic cells

For the preparation of synthetic cells, 18:1 (Δ9-*cis*) phosphatidylcholine (850375P, Avanti Polar Lipids) was mixed with mineral oil (M5904, Sigma-Aldrich) at a ratio of 0.1% w/v to prepare the oil phase by referring to the method of Kato et al.[37]. Then, 3 µl of the CFE reaction mixture was dropped into 40 µl of the oil phase. After gentle mixing, the turbid mixture (8 µl) was pipetted into the sealed slide chamber and loaded under the microscope at 30 °C to incubate the CFE reactions.

Statistics and reproducibility

Statistical analyses were performed using a Student's *t*-test (unpaired two-tailed) for comparison between two groups and a one-way analysis of variance (ANOVA) for multiple comparisons. Information regarding error bars and the number of biological replicates or samples is described in the corresponding figures. All experiments shown as independent experiments in the figure legends were biologically independent experiments. Unless specified, data presented in images, plots and charts are representative of two independent experiments.

Reporting summary

Further information on research design is available in the Nature Portfolio Reporting Summary linked to this article.

Data availability

All data that support the findings of this study are available within the paper and the Supplementary Information or from the corresponding authors. Source data are provided with this paper.

References

43. Stark, J. C. et al. BioBits™ Bright: a fluorescent synthetic biology education kit. *Sci. Adv.* **4**, eaat5107 (2018).
44. Gardner, T. S., Cantor, C. R. & Collins, J. J. Construction of a genetic toggle switch in *Escherichia coli*. *Nature* **403**, 339–342 (2000).
45. Huang, S. C. et al. Rational design and hierarchical assembly of a genetically engineered resilin–silk copolymer results in stiff hydrogels. *ACS Biomater. Sci. Eng.* **3**, 1576–1585 (2017).
46. Hong, K., Song, D. & Jung, Y. Behavior control of membrane-less protein liquid condensates with metal ion-induced phase separation. *Nat. Commun.* **11**, 5554 (2020).

Author contributions

X.-X.X., Z.-G.Q. and B.-T.J. conceptualized the project, designed the research and wrote the paper. B.-T.J. and H.-T.P. performed plasmid construction, cell-free protein expression, compartment imaging and characterization, analyzed the data and wrote the draft.

Competing interests

The authors declare no competing interests.

Additional information

Extended data is available for this paper at https://doi.org/10.1038/s41589-025-01840-4.

Supplementary information The online version contains supplementary material available at https://doi.org/10.1038/s41589-025-01840-4.

Correspondence and requests for materials should be addressed to Zhi-Gang Qian or Xiao-Xia Xia.

Peer review information *Nature Chemical Biology* thanks Yan Huang and the other, anonymous reviewer(s) for their contribution to the peer review of this work.

Reprints and permissions information is available at www.nature.com/reprints.
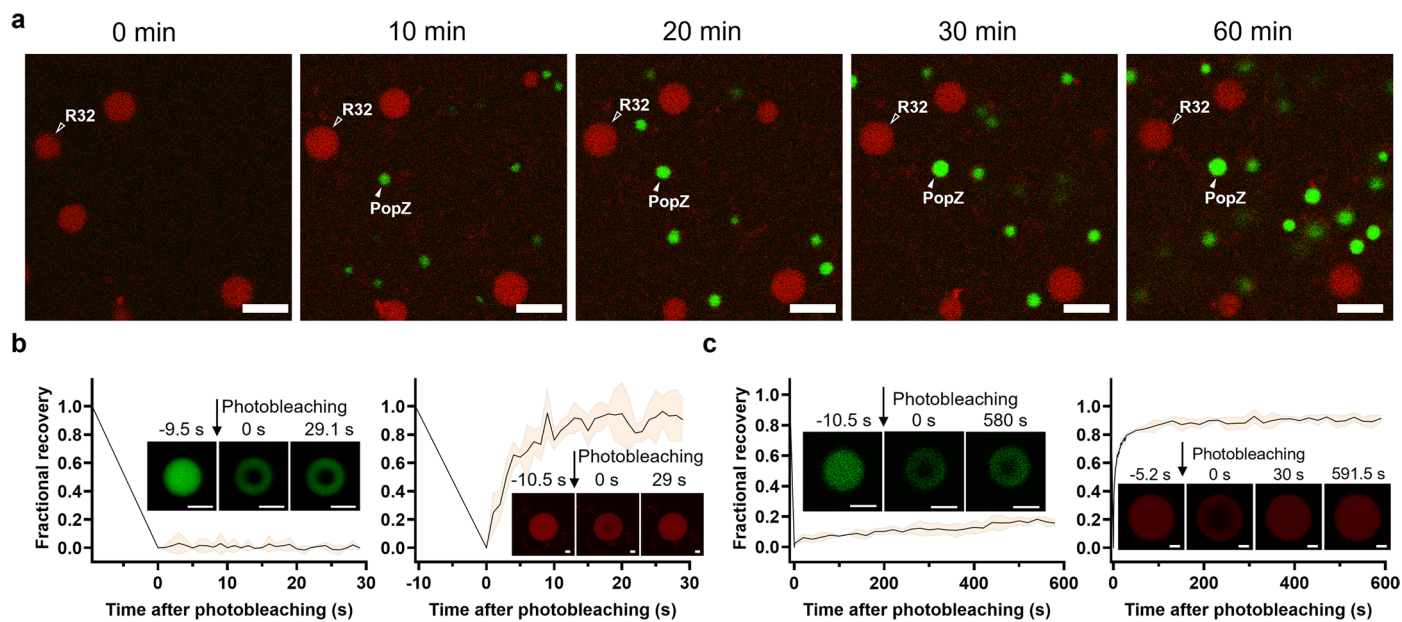
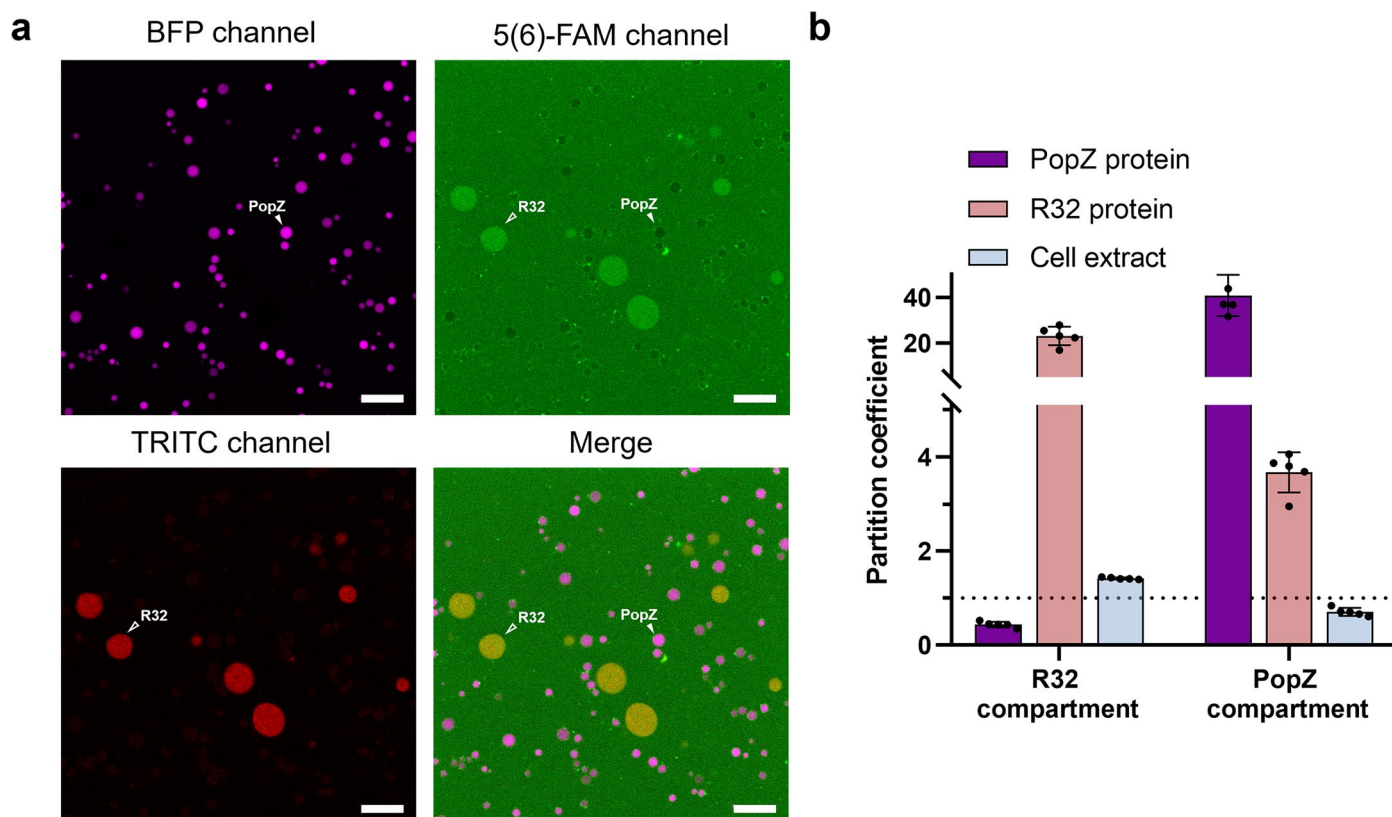**Extended Data Fig. 1 | Formation of compartment consortia and their dynamic properties. a**, Time-lapse imaging of exogenously added His-R32 and de novo expressed PopZ. The CFE mixture containing the same components as the experiment shown in Fig. 2b was incubated for the indicated times. Shown are the merged images from the GFP and TRITC channels, indicating the PopZ and His-R32 protein compartments, respectively. Scale bars, 10 μm. **b**, Fluorescence recovery after photobleaching (FRAP) of the PopZ (left) and His-R32 (right) compartments in the CFE system incubated at 30 °C for 20 min. Data are presented as mean ± s.d. of n = 4 compartments, and the insets show confocal images of bleaching on single compartments. **c**, FRAP of the PopZ (left) and His-R32 (right) compartments in the CFE system incubated at 30 °C for 240 min. Data are presented as mean ± s.d. of n = 3 compartments. Note that the data are derived from the same experiment shown in Fig. 2d. Scale bars in **b** and **c**, 2 μm. As *de novo* PopZ protein synthesis was rapid during the first 2 h of CFE incubation (Supplementary Fig. 2d), fluorescence recovery of the 20 min-compartments was monitored for a short time period of 30 s, whereas recovery of the 240 min-compartments was monitored for an extended time of about 600 s.
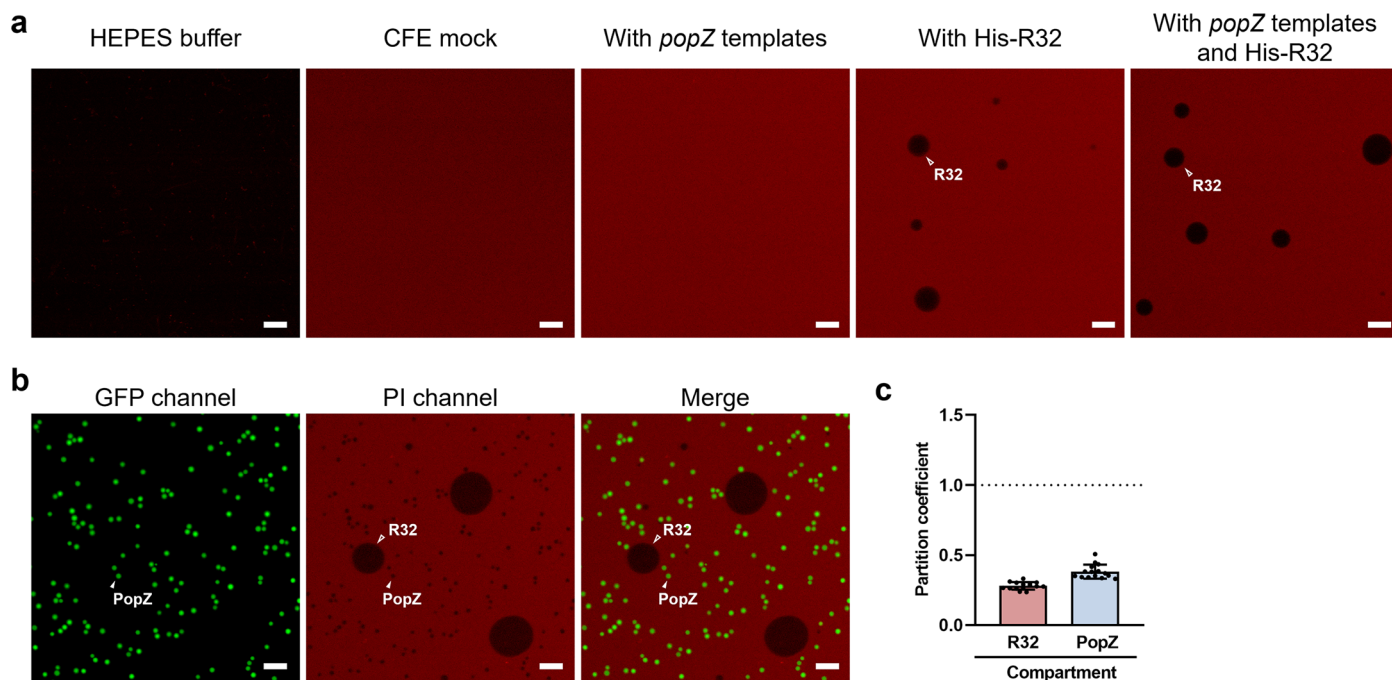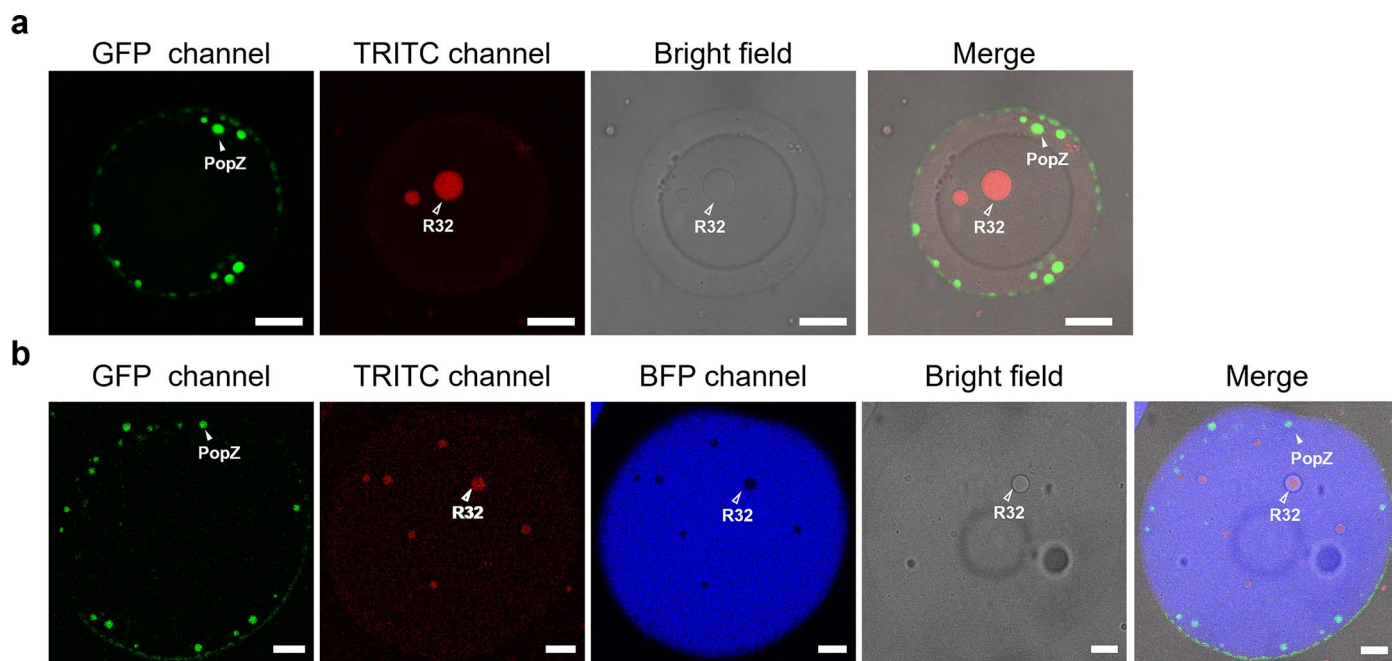
Extended Data Fig. 2 | The compartment consortia repel nucleic acids in the CFE system. a, Confocal images of propidium iodide (PI)-stained CFE mixtures with the addition of 10 mg mL^{-1} His-R32 (for R32 compartment formation), the *popZ* gene template spiked with its *gfpmut3* fusion or in combinations. The HEPES buffer used for mixture preparation, and the mock CFE mixture were included as controls. The *E. coli* cell extract-derived nucleic acids and gene templates were readily stained with PI (13.3 μM), revealing their even distribution in solution. **b**, Confocal images of the two populations of compartments formed after 4 h incubation of the CFE mixture at 30 °C. The emerging PopZ compartments and the R32 compartments did not mix with each other, and the synthetic compartment consortia were separated from their surrounding nucleic acids. Scale bars, 10 μm. **c**, Partition coefficient of nucleic acids, which is determined as the ratio of fluorescence intensity inside the compartment and the outside bulk phase, and presented as mean ± s.d. of $n = 15$ compartments. Data in **a-c** are representative of $n = 3$ independent experiments.

Extended Data Fig. 3 | The compartment consortia are not co-localized with the transcription and translation machinery proteins in the CFE system. a, Confocal images of the CFE mixture upon 4 h-incubation at 30 °C. Scale bars, 10 μm. The initial CFE mixture contained 5 mM Ni^{2+}, the *popZ* gene template spiked with *mTagBFP2* fusion at a molar ratio of 13.3:1, His-R32 spiked with its TRITC conjugate at a molar ratio of 10:1, the cell extract (33% v/v) and its 5(6)-FAM conjugate (7% v/v). **b**, Partition coefficients of the fluorescent protein components in the two populations of compartments, which are presented as mean ± s.d. of *n* = 5 compartments. Data in **a-b** are representative of *n* = 3 independent experiments.

a

b

Extended Data Fig. 4 | Construction of membraneless compartment consortia in protocells. a,b Confocal images of the two populations of compartments in the protocells that encapsulated the CFE mixtures without (**a**) and with (**b**) expression of the blue fluorescent protein mTagBFP2. The emulsion droplet-based protocells were prepared by dissolving (Δ9-Cis) phosphatidylcholine in mineral oil to encapsulate the CFE mixtures, which contained the *popZ* gene spiked with its *gfpmut3* fusion at a molar ratio of 13.3:1, His-R32 spiked with its TRITC conjugate at a molar ratio of 10:1, and 5 mM Ni²⁺. For additional expression of the reporter mTagBFP2 protein, 5 nM of the *mTagBFP2* gene was supplemented into the CFE system. All protocells were incubated at 30 °C for 4 h before confocal imaging. Scale bars, 10 μm. The expressed reporter protein mTagBFP2 produced blue fluorescence dispersed through the protocell cytosol, whereas the PopZ protein formed droplet-like compartments that are mostly localized to the lipid membrane, indicating that the membrane surface may have a role in promoting PopZ condensate nucleation and membrane localization. Data in **a-b** are representative of *n* = 2 independent experiments.
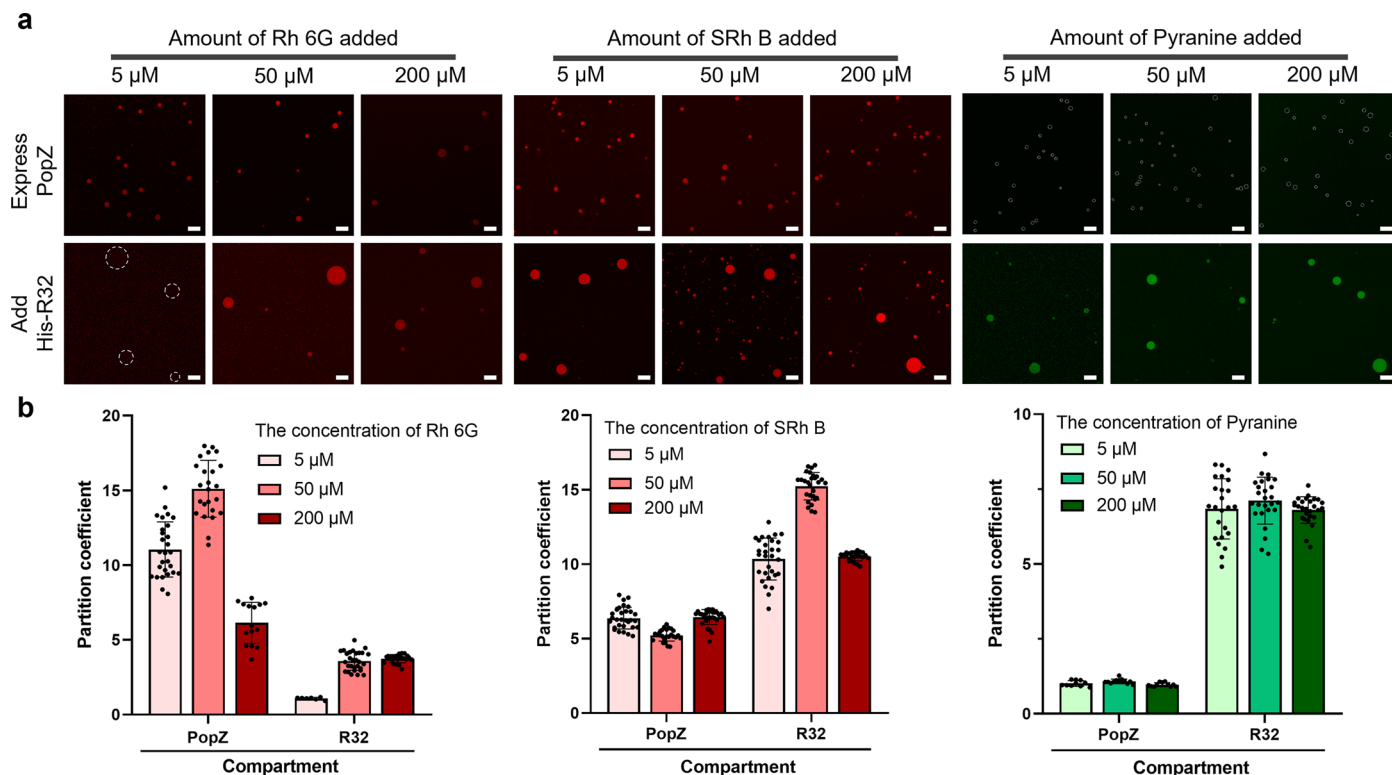
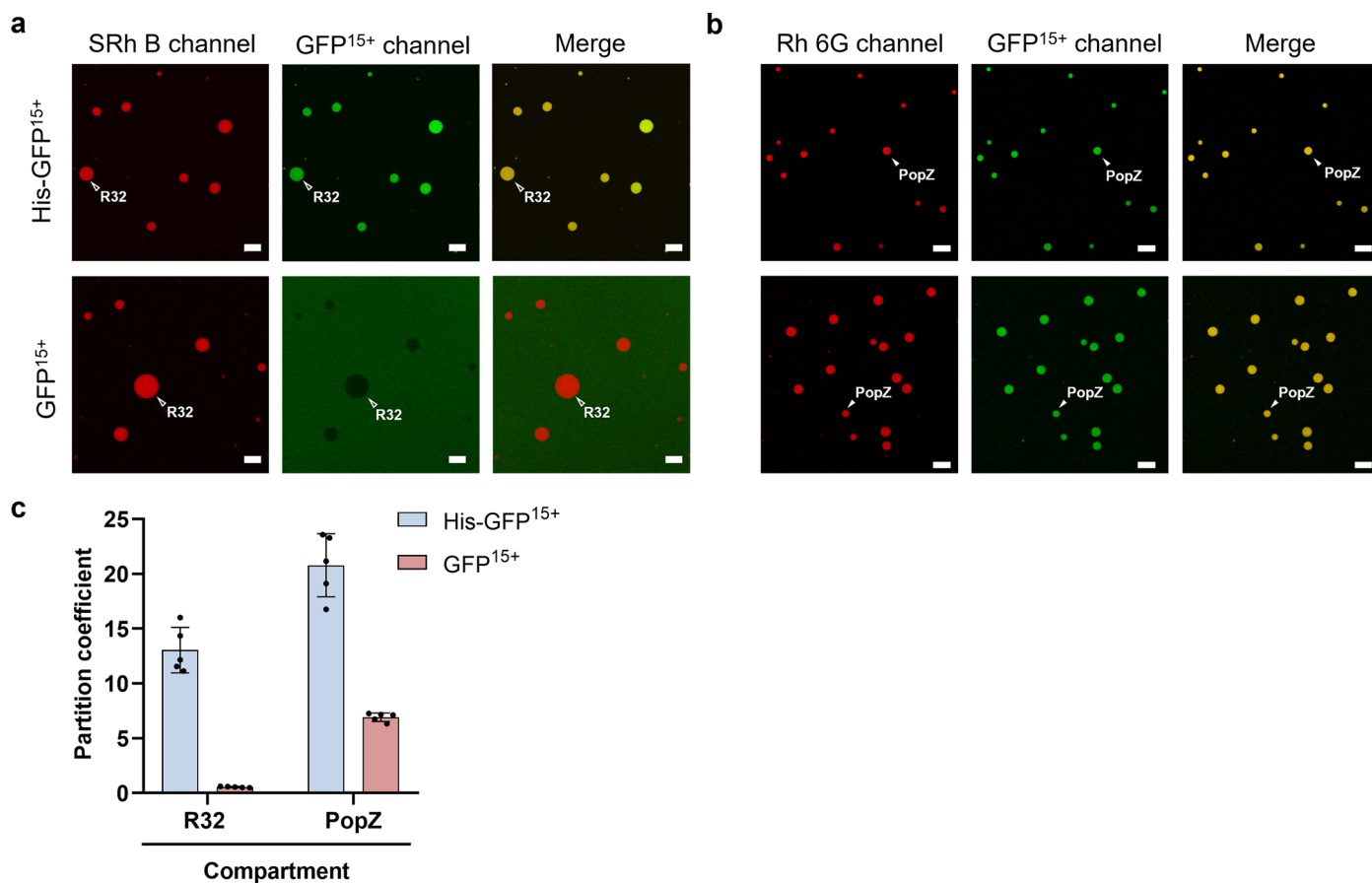**Extended Data Fig. 5 | Selective partitioning of small molecules in a single population of compartments. a**, Confocal images of the PopZ (top) and R32 (bottom) compartments in the CFE mixtures. A fluorescent molecule was added at the indicated concentrations. The mixtures containing the *popZ* gene (10.55 nM) were incubated at 30 °C for 4 h to form the PopZ compartments. Alternatively, 10 mg mL^{-1} His-R32 and 5 mM Ni^{2+} were included for R32 compartment formation. For clarity, the weakly stained compartments were circled with dotted lines. Scale bars, 10 μm. **b**, Partition coefficient of Rh 6 G (left), SRh B (middle), and pyranine (right) in the respectively compartments. Data are presented as mean ± s.d. with *n* = 28, 24, 15, 7, 29, 23 compartments in Rh 6 G partition (left), 30, 25, 30, 30, 28, 23 in SRh B partition (middle), and 10, 12, 11, 24, 26, 27 in pyranine partition (right), respectively.

a

b
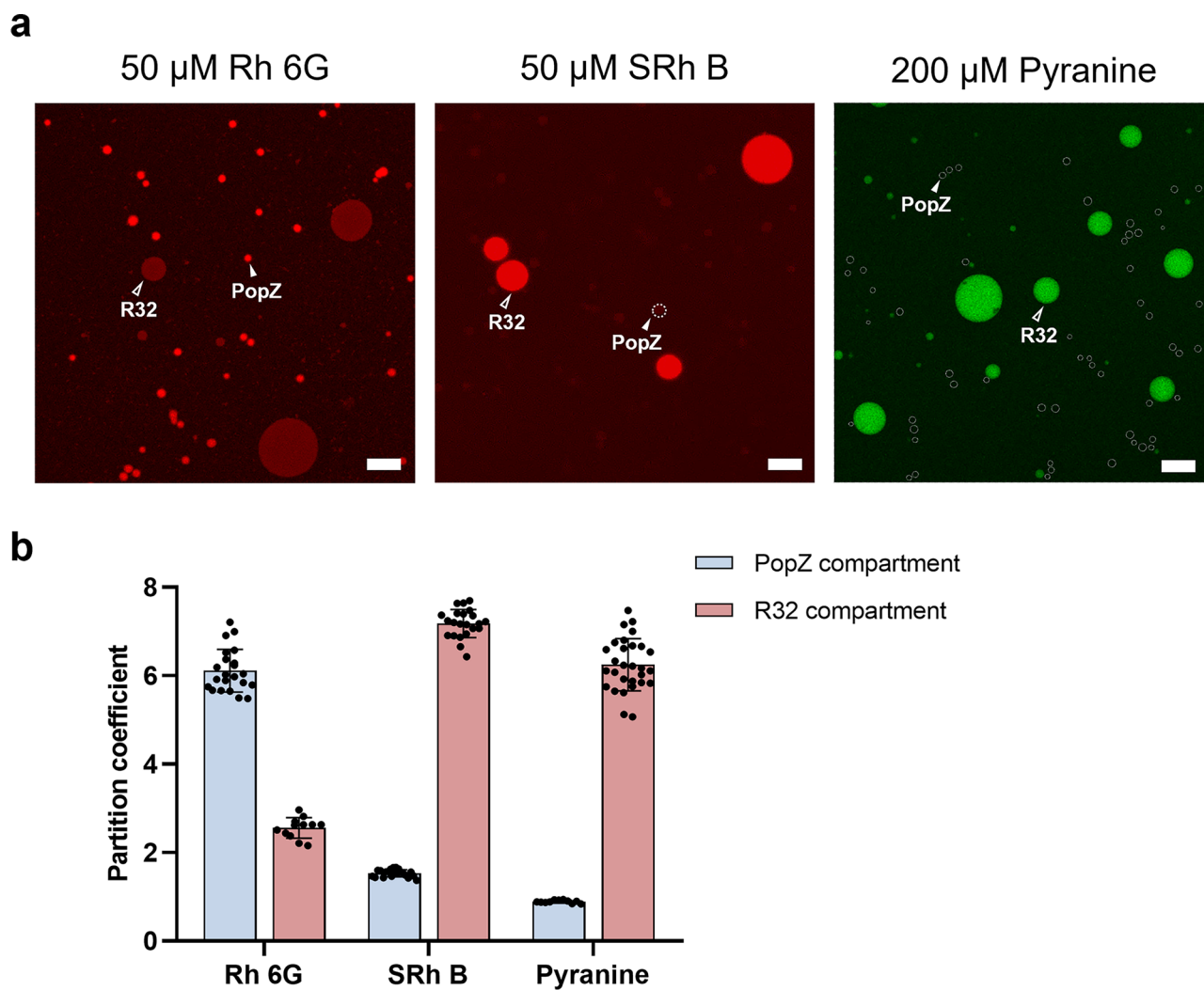
Extended Data Fig. 6 | Selective enrichment of fluorescent molecules by the compartment consortia. a, Confocal images of the compartment consortia in the CFE mixtures. The initial mixtures, which contained one fluorescent molecule (50 µM SRh B, 50 µM Rh 6 G or 200 µM Pyranine), 10.55 nM of the *popZ* gene, 10 mg mL^{-1} His-R32, and 5 mM Ni^{2+}, were incubated at 30 °C for 4 h to form the binary population of PopZ and R32 compartments. For clarity, the weakly stained compartments were circled with dotted lines. Scale bars, 10 µm. **b**, Partition coefficient of the fluorescent dye in the respective compartments at 4 h post-incubation of the CFE mixtures (pseudo-steady state). Data are presented as mean ± s.d. with n = 22 and 12 compartments for the Rh 6 G partition, 21 and 22 for the SRh B partition, 11 and 29 for the pyranine partition, respectively.

Extended Data Fig. 7 | Distinct partitioning of cargo GFP[15+] and its precursor (His-GFP[15+]) into compartments. Confocal images of His-GFP[15+] (top) and GFP[15+] (bottom) partitioning within the R32 compartments (**a**) and PopZ compartments (**b**). Addition of His-R32 at 10 mg mL^{−1} into the initial CFE mixtures yielded the R32 compartments, whereas addition of the *popZ* gene (10.55 nM) led to the formation of PopZ compartments. The CFE mixtures contained 5 mM Ni^{2+} and

4.77 nM of the corresponding *His-GFP[15+]* gene or *GFP[15+]* gene, and the reactions were carried out at 30 °C for 4 h. SRh B (5 μM) or Rh 6 G (50 μM) was used to stain the compartments for imaging. Scale bar, 10 μm. **c**, Partition coefficients of the green fluorescent protein in the two populations of compartments, which are presented as mean ± s.d. of *n* = 5 compartments. Data in **a-b** are representative of *n* = 3 independent experiments.

a

Before communication

b

c
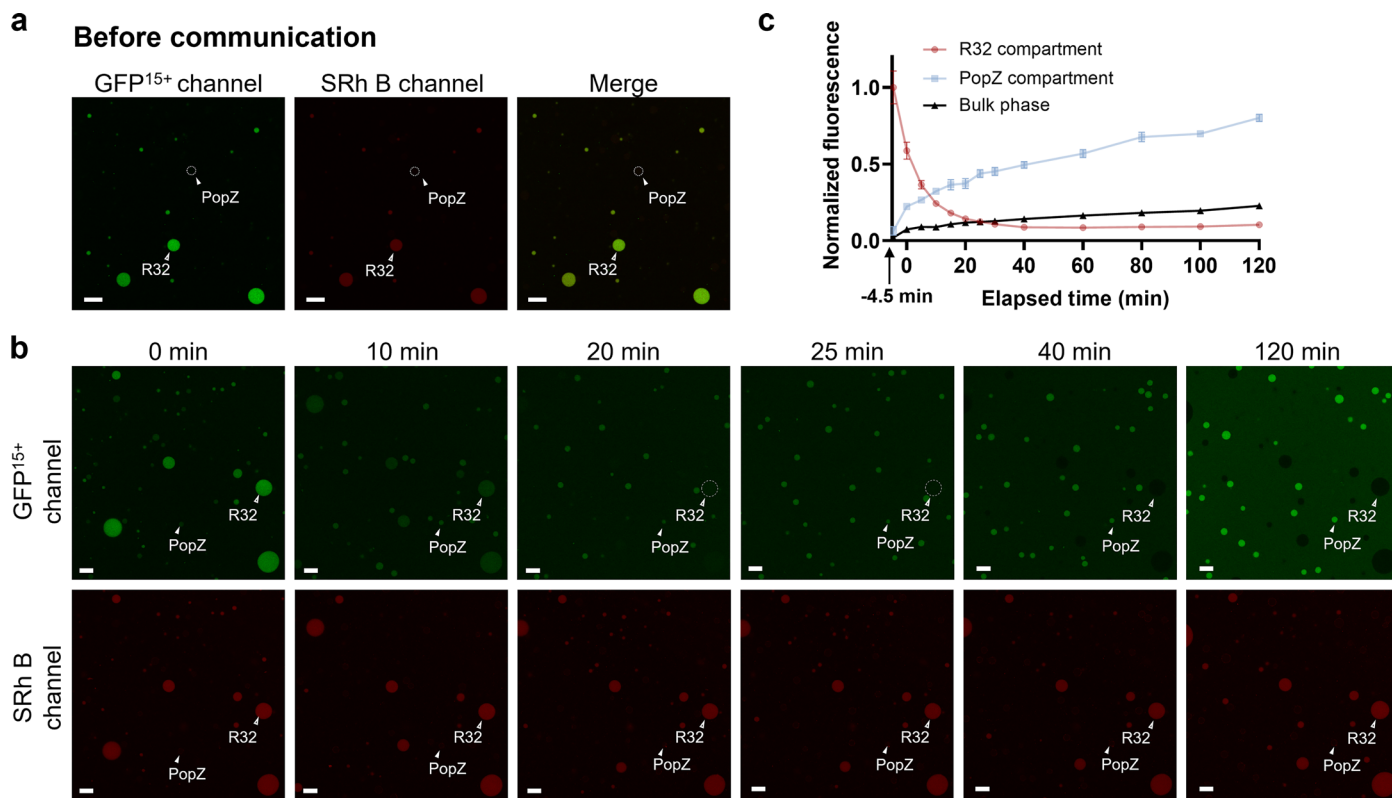
Extended Data Fig. 8 | Kinetics of protein cargo communication. a, Confocal images of the compartment consortia before the addition of the communication trigger (TEV protease). The CFE mixtures containing 10 mg mL⁻¹ His-R32, 5 mM Ni²⁺, and 5 μM SRh B had been incubated at 30 °C for 2 h to generate His-tagged GFP¹⁵⁺, followed by 4 h-expression of the *popZ* gene to form the coexisting PopZ compartments. The targeting sequence (His tag) allowed tagged GFP¹⁵⁺ to be mostly accumulated in the 'sender' R32 compartments before fluorescent protein communication. **b**, Time-lapse fluorescence imaging of protein communication upon addition of 8.82 μM TEV protease. Scale bars, 10 μm. **c**, Quantification of fluorescent protein in the sender R32, receiver PopZ compartments, and the bulk phase as a function of elapsed time under confocal imaging. The fluorescence intensities were normalized by setting the fluorescence intensity of the sender compartment before communication to 1. Data are presented as mean±s.d. of *n* = 5 compartments. The arrow indicates the offset processing time of the sample, *ca*. 4.5 min which is required for loading sample into the slide chamber and operating the confocal microscope before image acquisition. Note that slight accumulation of the cargo protein in the bulk phase occurred, which is attributed to incomplete capture of the released cargo by the receiver compartments.
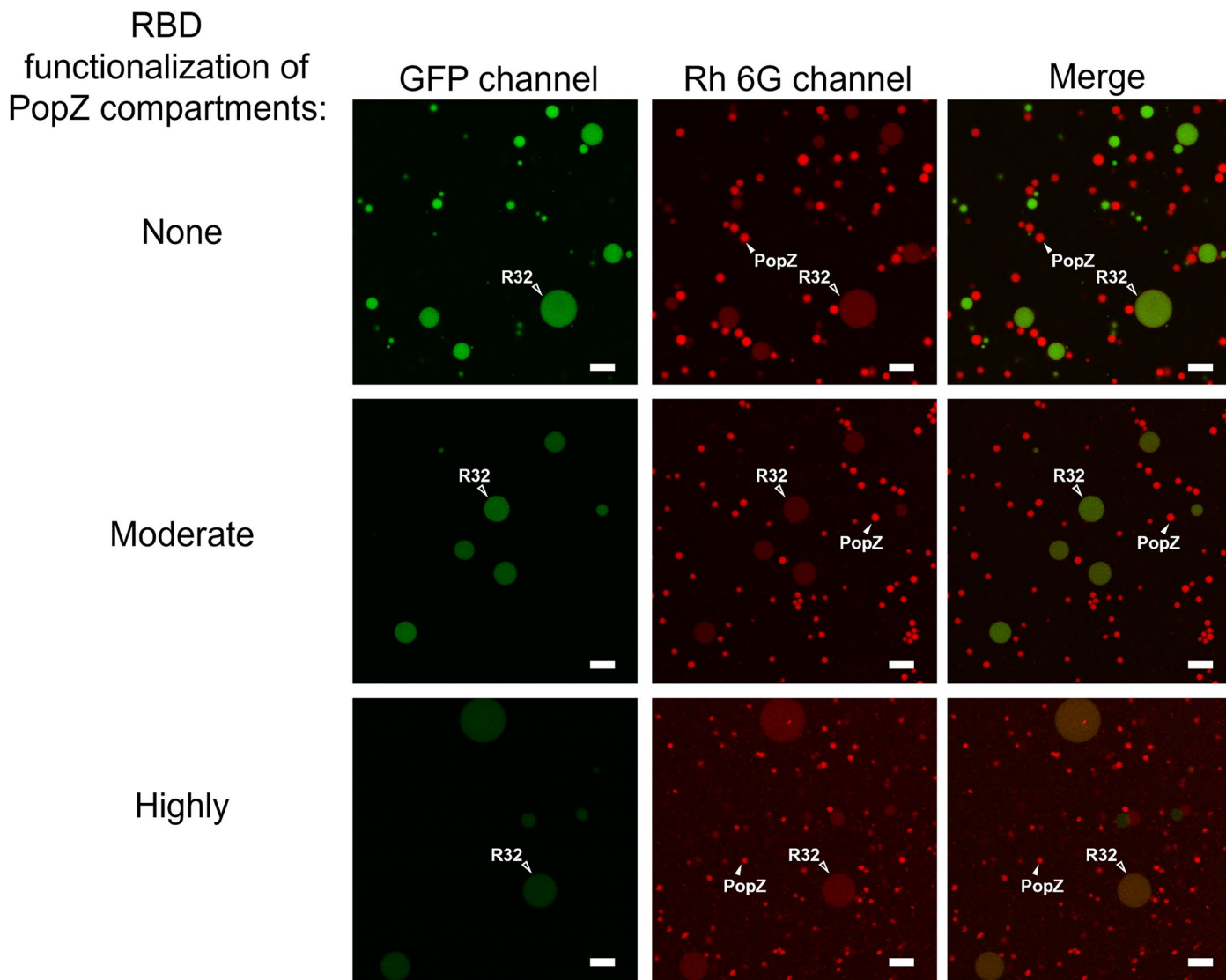
Extended Data Fig. 9 | RBD-functionalized PopZ compartments attenuated the localized reporter protein in the receiver R32 compartments. Confocal fluorescence images of the compartment consortia. The controller PopZ compartments with varied functionalization degrees emerged from CFE of the *popZ* gene (none), *popZ-RBD* fusion gene (highly) or their mixture in a 1:1 ratio (moderate). The CFE systems also contained the DNA template (4.90 nM) encoding the histidine-tagged GFPmut3 reporter protein, 50 μM Rh 6 G, 10 mg mL^{-1} His-R32 protein and 5 mM Ni^{2+} to form the receiver compartments. Scale bars, 10 μm. Data are representative of n = 2 independent experiments.
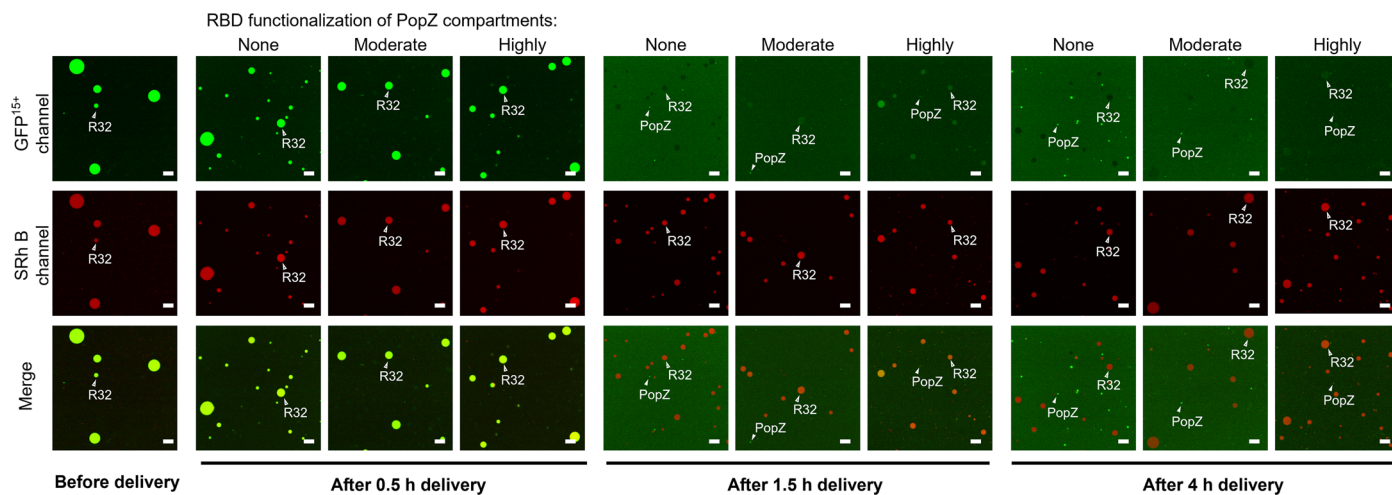
Extended Data Fig. 10 | Fluorescence images of the compartment consortia before and after programmed delivery of the cargo protein GFP[15+]. The precursor cargo was synthesized from the *His-linker-TEVs-gfp[15+]* gene by CFE at 30 °C for 2 h in the initial mixtures that also contained 10 mg mL^{-1} His-R32, 5 mM Ni^{2+} and 5 µM SRh B. The necessary *popZ* templates and 2.43 nM of the *His-TEV protease* gene were added as DNA triggers into the CFE systems for incubation for additional 0.5 to 4 h. The PopZ compartments with varied RBD functionalization degrees emerged from CFE of the *popZ* gene (none), *popZ-RBD* fusion gene (highly) or their mixture in a 1:1 ratio (moderate). For clarity, the brightness and contrast of the images were adjusted. Note that the GFP channel images before and after 4 h triggered delivery were the same as those shown in Fig. 5d–g. Scale bars, 10 µm. Data are representative of *n* = 2 independent experiments.

nature portfolio

Corresponding author(s):   Xiao-Xia Xia, Zhi-Gang Qian

Last updated by author(s):   Nov 20, 2024

Reporting Summary

Nature Portfolio wishes to improve the reproducibility of the work that we publish. This form provides structure for consistency and transparency in reporting. For further information on Nature Portfolio policies, see our Editorial Policies and the Editorial Policy Checklist.

Statistics

For all statistical analyses, confirm that the following items are present in the figure legend, table legend, main text, or Methods section.

n/a	Confirmed	
☐	☒	The exact sample size (*n*) for each experimental group/condition, given as a discrete number and unit of measurement
☐	☒	A statement on whether measurements were taken from distinct samples or whether the same sample was measured repeatedly
☐	☒	The statistical test(s) used AND whether they are one- or two-sided *Only common tests should be described solely by name; describe more complex techniques in the Methods section.*
☒	☐	A description of all covariates tested
☐	☒	A description of any assumptions or corrections, such as tests of normality and adjustment for multiple comparisons
☐	☒	A full description of the statistical parameters including central tendency (e.g. means) or other basic estimates (e.g. regression coefficient) AND variation (e.g. standard deviation) or associated estimates of uncertainty (e.g. confidence intervals)
☐	☒	For null hypothesis testing, the test statistic (e.g. *F*, *t*, *r*) with confidence intervals, effect sizes, degrees of freedom and *P* value noted *Give P values as exact values whenever suitable.*
☒	☐	For Bayesian analysis, information on the choice of priors and Markov chain Monte Carlo settings
☒	☐	For hierarchical and complex designs, identification of the appropriate level for tests and full reporting of outcomes
☒	☐	Estimates of effect sizes (e.g. Cohen's *d*, Pearson's *r*), indicating how they were calculated

Our web collection on statistics for biologists contains articles on many of the points above.

Software and code

Policy information about availability of computer code

Data collection	SDS-PAGE: Microtek Bio-5000 Plus scanner Confocal imaging and FRAP: Leica TCS SP8 STED 3X microscope Fluorescence measurements: Spark multimode microplate reader MALDI-TOF mass spectra: Bruker ultrafleXtreme Protein content determination: Nano drop 2000
Data analysis	Leica Application Suite X (LAS X) 3.7.1.21655 for confocal image analysis Image J 1.53e and Microsoft Excel 2021 for partition coefficient analysis Origin 2017 for curve fitting

For manuscripts utilizing custom algorithms or software that are central to the research but not yet described in published literature, software must be made available to editors and reviewers. We strongly encourage code deposition in a community repository (e.g. GitHub). See the Nature Portfolio guidelines for submitting code & software for further information.

Data

All manuscripts must include a data availability statement. This statement should provide the following information, where applicable:

- Accession codes, unique identifiers, or web links for publicly available datasets
- A description of any restrictions on data availability
- For clinical datasets or third party data, please ensure that the statement adheres to our policy

> All data supporting the findings of this study are available within the article and its supplementary files. All raw images that support the findings of this study can be directed to, and will be fulfilled by, the corresponding authors. Source data are provided with this paper.

Human research participants

Policy information about studies involving human research participants and Sex and Gender in Research.

Reporting on sex and gender	Not applicable
Population characteristics	Not applicable
Recruitment	Not applicable
Ethics oversight	Not applicable

Note that full information on the approval of the study protocol must also be provided in the manuscript.

Field-specific reporting

Please select the one below that is the best fit for your research. If you are not sure, read the appropriate sections before making your selection.

☒ Life sciences ☐ Behavioural & social sciences ☐ Ecological, evolutionary & environmental sciences

For a reference copy of the document with all sections, see nature.com/documents/nr-reporting-summary-flat.pdf

Life sciences study design

All studies must disclose on these points even when the disclosure is negative.

Sample size	Sample size for each experiment is indicated in figures or figure legends. The sample sizes were not predetermined by statistical tools, sample or group sizes of the experiments chosen are based on previous experience in the lab and other similar studies (PMID: 332601486; 37973891; 36747054).
Data exclusions	Data were not excluded from analysis.
Replication	All experiments were independently repeated at least two times and all attempts to replicate the experiments were successful.
Randomization	Randomization was not applicable because all samples were treated similarly.
Blinding	The study is not blinded as the experiments and analysis were performed by the same group of researchers.

Reporting for specific materials, systems and methods

We require information from authors about some types of materials, experimental systems and methods used in many studies. Here, indicate whether each material, system or method listed is relevant to your study. If you are not sure if a list item applies to your research, read the appropriate section before selecting a response.

Materials & experimental systems

n/a	Involved in the study
☒	☐ Antibodies
☒	☐ Eukaryotic cell lines
☒	☐ Palaeontology and archaeology
☒	☐ Animals and other organisms
☒	☐ Clinical data
☒	☐ Dual use research of concern

Methods

n/a	Involved in the study
☒	☐ ChIP-seq
☒	☐ Flow cytometry
☒	☐ MRI-based neuroimaging